

# NATIONAL TRANSPORTATION SAFETY BOARD

Office of Research and Engineering  
Materials Laboratory Division  
Washington, D.C. 20594



June 29, 2007

MATERIALS LABORATORY STUDY

Report No. 07-063

---

## A. ACCIDENT

Place : Boston, Massachusetts  
Date : July 10, 2006  
Vehicle : I-90 Connector Tunnel to Ted Williams Tunnel  
NTSB No. : HWY06MH024  
Investigator : Mark Bagnard

## B. TOPICS ADDRESSED

Finite element analysis was used to study the deformation of the materials that constitute an adhesive anchor, and to investigate the effect of voids in the adhesive.

## C. DETAILS OF THE STUDY

In examining the anchors and anchor holes from the tunnel ceiling support system, voids within the epoxy adhesive were observed, as documented in Materials Laboratory Factual Report 06-091. These voids often extended over the full embedded length of the threaded rod and eliminated the adhesion between the anchor and the concrete over a substantial portion of the interfacial surface area (on the order of 25 percent). Finite element modeling was used to investigate the effect of voids within the epoxy adhesive on the stress and strain fields in the anchor system. All of the finite element modeling was performed using ABAQUS version 6.6.

### Model Description

Both two-dimensional axisymmetric and three-dimensional models were used to investigate the deformation in the epoxy. The overall model geometry was the same for each model. A cylinder of concrete 7 inches in diameter and 8.5 inches tall was modeled. The hole in the concrete was 0.75 inches in diameter and 5.5 inches deep. The length of the anchor modeled was 5 inches, and the anchor was inserted 5 inches deep into the hole in the concrete, so the bottom of the anchor was flush with the surface of the concrete cylinder. In the installation in the tunnels, a red polyethylene cap was inserted into each hole in the concrete before the anchor was installed into the hole. The epoxy did not bond to the polyethylene cap, so the epoxy was modeled as beginning 0.542 inches from the open end of the hole to model the lack of bond to the cap. The bonded length of the

anchor was therefore 4.458 inches. The overall model geometry is sketched in figure 1, with an oblique view in figure 2.

Displacements were held at zero along the outer cylindrical surface and the top surface of the concrete. Mirror symmetry boundary conditions were imposed on the midplane surfaces of the anchor, the epoxy and the concrete, as indicated in figure 2. A uniform downward tensile stress of 10 ksi was imposed on the bottom end of the anchor, which is equivalent to a force of 2,051 pounds.

A two-dimensional axisymmetric model of the anchor necessarily eliminates the helical geometry of the threads on the anchor. The helical geometry of the threads was also eliminated from the three-dimensional model in order to make use of mirror symmetry, for comparison with the two-dimensional model and to simplify the geometry description and mesh generation. The helical geometry of the threads was considered to be less important than the local geometry of the thread profile. The thread profile used for the model of the anchor is indicated in figure 3. This thread profile was based on measurements from an anchor from the accident site; the profile is within the specification for 5/8-11 UNC (Unified Coarse) screw threads [1], which have a nominal outer diameter of 5/8 inch and 11 threads per inch. The thread geometry shown in figure 3 has sharp corners. The interior and exterior corners on the threads on the anchor were measured as having an average radius of approximately 0.002 inches. The mesh used for the axisymmetric models was fine enough to incorporate the rounded thread profile. The solid models required a coarser mesh and used the thread geometry with sharp corners.

Six different model variants are discussed in this report. Two interactions between the anchor and the epoxy were studied, one being a tie constraint (simulating perfect adhesion) and the second a frictionless contact condition (which allows only mechanical interlocking). These two conditions were used as bounds on the possible range of interactions between the anchor and the epoxy. The post-accident examination of the anchor holes indicated that the anchors separated cleanly from the epoxy at the top end of each hole, suggesting that the bonding between the epoxy and the anchor was relatively weak in direct tension (see Materials Laboratory Factual Report 06-091). In all cases, a perfect bond was assumed to exist between the epoxy and the concrete, with a tie constraint imposed at the interface. For each type of anchor/epoxy interaction, an axisymmetric model and four solid models (two with voids and two without) were studied. The solid models generally required a much coarser mesh than the axisymmetric models to cover the complete time history under examination.

In the three-dimensional models that included a void, the epoxy was removed from a wedge of 45 degrees adjacent to the plane of mirror symmetry. With the symmetry boundary condition imposed, this wedge is doubled to model a void in a wedge of 90 degrees, to mimic a void having an interfacial area fraction of 25 percent. Cutaway views of the geometry of the solid models (with and without a void) are shown in figure 4. In one model, epoxy completely fills the gap between the anchor and the concrete cylinder (above the area where there was a red polyethylene cap installed in the tunnel). The image on the right shows the 45-degree wedge of epoxy removed to simulate a void.

## Material Properties

Given that the exact material properties have not been measured, estimated values for the stiffness of each material were used. The stiffness properties of the different materials span several orders of magnitude, so order of magnitude estimates were used based on typical properties for steel, concrete and epoxy.

Both the anchor and the concrete roof section were modeled as isotropic linearly elastic materials. The anchor was modeled as steel having a Young's modulus of 30,000 ksi and a Poisson's ratio of 0.3. The concrete was specified to have a Young's modulus of 3,000 ksi and a Poisson's ratio of 0.17. The compressive strength  $f'_c$  of the concrete in the tunnel roof was specified to be 4000 psi; Young's modulus  $E$  of typical concrete can be roughly related to the compressive strength as  $E$  (in psi) =  $57,000\sqrt{f'_c}$  (where  $f'_c$  is also taken to be in psi) [2].

The epoxy was modeled as an isotropic linearly viscoelastic material. ABAQUS allows for the input of time-dependent (or frequency-dependent) shear and bulk moduli. The initial (glassy) value of Young's modulus for the epoxy was specified to be 300 ksi. The initial value of Poisson's ratio was specified to be 0.3, based on information from the literature [3]. Additional cases assuming the epoxy was nearly incompressible with an initial Poisson's ratio of 0.49 were also examined, based on the possibility that the fillers increased the initial bulk modulus substantially but had little effect on the shear modulus or Young's modulus. With these parameters, the initial value of the shear modulus would be  $G_0 = 115$  ksi. The time-dependent shear modulus was specified by a Prony series as

$$G(t) = G_{\infty} + \sum_{i=1}^n G_i \exp\left(\frac{-t}{\tau_i}\right) \quad (1)$$

where  $G_{\infty}$  is the rubbery, long-time asymptotic value of the shear modulus,  $G_i$  is the magnitude of the change in the shear modulus associated with each characteristic relaxation time  $\tau_i$ . The initial value of the shear modulus (at  $t = 0$ ) is given by

$$G_0 = G_{\infty} + \sum_{i=1}^n G_i \quad (2)$$

For this investigation, the goal was to compare results from the different models, so the exact time dependence of the relaxation behavior of the epoxy was not of interest. Consequently, only a single relaxation time was used in the model (in this case equal to one time unit), with the shear modulus therefore given by

$$\begin{aligned} G(t) &= G_{\infty} + G_1 \exp(-t) \\ &= G_{\infty} + (G_0 - G_{\infty}) \exp(-t) \end{aligned} \quad (3)$$

For real polymers, relaxation behavior generally occurs over a much broader spectrum of relaxation times, so an accurate representation of the true relaxation behavior would require a number of terms (ten or more) in equation (1). The rubbery shear modulus was taken to be two orders of magnitude less than the glassy shear modulus, so  $G_{\infty} = (0.01)G_0$ . Equation (3) indicates how the shear modulus would decay in a stress relaxation

experiment, where a sudden deformation is imposed and then held constant, while the stress decreases exponentially. The shear creep compliance  $J(t)$  would describe how the epoxy would respond in creep, with a sudden stress imposed leading to a steadily increasing deformation. The shear creep compliance is related to the shear modulus through a convolution integral, so the compliance is not simply the inverse of the modulus, except at very short or very long times. The initial glassy value of the shear creep compliance is equal to the inverse of the glassy value of the shear modulus, with  $J_0 = 1/G_0$ , and the final rubbery value of the shear creep compliance is equal to the inverse of the rubbery shear modulus, with  $J_\infty = 1/G_\infty$ . For a modulus with a single relaxation time as in equation (3), the compliance can be expressed as a similar function that also has a single time parameter, but the time constant of the compliance is  $G_0/G_\infty$  longer than the time constant of the relaxation function [3]. In this case,  $G_0/G_\infty = 100$ , so the time for the compliance to increase from the glassy value to the rubbery value is 100 time units. With these parameters, the compliance increases by about a factor of 10 after 10 time units, increases by about a factor of 40 after 50 time units and increases by about a factor of 60 after 100 time units.

The bulk modulus of the epoxy was held constant over time. There is limited data regarding the relaxation behavior of the bulk modulus, and an assumption that the bulk modulus is a constant is not uncommon [3]. Some data exist showing that the bulk modulus decreases by only a factor of 2 compared to a decrease in the shear modulus by a factor of 100 or more [4]. Also, the inorganic fillers in the epoxy would serve to decrease the time-dependent behavior of the bulk modulus even further.

### Mesh Geometry

Linear (axisymmetric or solid) elements with reduced integration were used for all parts. Elements with a hybrid formulation intended for use with nearly incompressible materials were specified for the epoxy, since the shear modulus will decrease over time compared to the bulk modulus, leading to a more incompressible material behavior. Figure 5 shows a representative view of the mesh used for the axisymmetric models. The axisymmetric models used 19,319 elements for the steel anchor, 163,804 elements for the epoxy adhesive layer and 336 elements for the concrete. The solid models were substantially coarser. All of the solid models used 37,219 elements for the steel anchor and 5,504 elements for the concrete, with the elements swept in wedges of approximately 10 to 15 degrees around the 180-degree circumference. In the solid models, 46,575 elements were used for the epoxy adhesive with a void and 52,571 elements were used for the epoxy adhesive with no void. A representative view of the mesh used for the solid models is shown in figure 6.

### Model Loading

Two steps were used to explore the stress and strain distributions in the epoxy. Both steps were quasistatic (there are no dynamic effects in the model), so the time scales for each step are arbitrary. In the first step, all of the materials were modeled as linearly

elastic to obtain the initial, glassy response of the epoxy. The second step was a viscoelastic step that included the time-dependent behavior of the epoxy. The time scale of the viscoelastic step is scaled by the relaxation times used in the Prony series of equation (1). In this case, only a single relaxation time with a scale of 1 time unit was used. In the two-dimensional axisymmetric models, the second step had a duration of 100 time units, while in the three-dimensional models, the second step was shortened to 50 time units.

## Results and Discussion

Displacements of the anchors are plotted in figures 7 through 10. For the axisymmetric models and the models without voids, symmetry allows for displacements only in the vertical direction. The vertical displacement of the bottom end of the anchor is shown in figure 7 for the axisymmetric models, indicating that the initial elastic displacement is similar for the two models but that the displacement increases at a greater rate for the model with only contact between the anchor and the epoxy than for the model with a tie constraint. Figure 8 compares the vertical anchor displacements from the models with the tie constraint between the anchor and the epoxy, showing that the solid model with no void gives similar results to the axisymmetric model for this condition. Figure 9 compares the vertical anchor displacements from the models with a contact interaction between the anchor and the epoxy. The solid model with no void shows a slightly larger displacement than the axisymmetric model, which arises in the initial elastic loading step, and then continues as an approximately constant offset through the second viscoelastic step. This offset beginning in the initial loading step is apparently a result of deeper interpenetration allowed in the contact by the coarser mesh in the solid model. For the models with voids, displacements along two axes (in the plane of mirror symmetry) are possible. Horizontal anchor displacements from the models with voids are shown in figure 10. In the model with a void and a tie constraint between the anchor and the epoxy, the lack of tension on the anchor in the area of the void allows for a small counterclockwise rotation with the bottom end of the anchor displacement away from the void. In the model with a void and a frictionless contact condition between the anchor and the epoxy, the open space of the void allows the anchor to slide in that direction and also to rotate first clockwise (as the bottom end of the anchor slides) then counterclockwise (after about 10 time units) as the top end of the anchor begins to overtake the bottom end.

For a typical brittle epoxy, fracture initiation could be characterized by a critical maximum principal strain, which, when positive, indicates the maximum direct tensile deformation of the material. Maximum principal strains are examined in figures 11 through 18. In the initial elastic step, when the epoxy responds as a glassy material, the maximum principal strains occur in the first or second thread roots near the free surface of the epoxy at the lower end of the anchor. Figure 11 shows contours of maximum principal strains for the axisymmetric models at the end of the initial elastic step. As time progresses through the second (viscoelastic) step, the epoxy softens, and the location of the maximum principal strain shifts from the lower end of the anchor to the thread root at the top end of the anchor. For all models, this transition takes place at about 10 time units in the second step. Figure 12 shows contours of maximum principal strains for the axisymmetric models after 50 time units in the second step. In the model with a tie constraint between the

anchor and the epoxy, the maximum principal strains are concentrated at both the top and bottom corners of the thread root, with a slightly larger strain concentration at the top corner of the thread root. In the model with a contact interaction between the anchor and the epoxy, the maximum principal strains are concentrated at the bottom surface of the thread at the corner of the thread root, and are substantially higher than the maximum strains in the model with the tie constraint between the anchor and the epoxy. The maximum principal strain concentrations in the solid models appear in similar locations with respect to the thread roots as those in the axisymmetric models, but they are not as large or as well resolved owing to the coarser mesh used for the solid models.

Figure 13 shows the evolution over time of the maximum principal strains in the epoxy from thread roots at the top and bottom of the anchor as calculated using the axisymmetric models. Figure 14 plots the same data as in figure 13, but on logarithmic scales to show more clearly the transition of the maximum principal strains from the bottom of the anchor to the top at about 10 time units.

Table 1 lists the maximum principal strains in the epoxy adhesive at various times as calculated by models with a tie constraint between the anchor and the epoxy. As noted above, the location of the maximum principal strain shifts from the bottom of the anchor to the top of the anchor at about 10 time units for all models. Although the anchor displacement calculated by the coarse solid model with no void matches that of the axisymmetric model (see figure 8), the maximum principal strains from the solid model are only about half the maximum principal strains from the axisymmetric model. In the initial elastic step (time = 1), the maximum principal strain in the solid model with a void is about 42 percent higher than that from the corresponding solid model with no void, so the increase is somewhat larger than the 33 percent increase that would be expected for the increase in the average strain in the epoxy when one quarter of the epoxy is removed to create the void. At longer times, the maximum principal strains in the solid models with and without voids tend to similar values, even though there are higher *average* stresses and strains in the epoxy in the model with the void.

Table 1. Maximum principal strains in the epoxy for models with a tie constraint between the anchor and the epoxy.				
Time	Axisymmetric	Solid No Void	Solid With Void	
			Edge of Void	Symmetry Plane
1	6.704e-3	4.232e-3	6.011e-3	3.571e-3
10	3.277e-2	1.927e-2	2.529e-2	2.080e-2
20	6.434e-2	3.376e-2	3.890e-2	3.634e-2
50	1.529e-1	8.015e-2	8.221e-2	7.820e-2
100	2.638e-1			

Figures 15 and 16 compare the maximum principal strains as functions of time for models with a tie constraint between the anchor and the epoxy. Figure 15 plots the maximum principal strains in the thread root at the top of the anchor, and figure 16 plots the maximum principal strains in the thread root at the bottom of the anchor. Comparing the two figures shows that the maximum principal strains at the top and bottom of the anchor are more similar in the model with the void than in the other two models.

Table 2 lists the maximum principal strains in the epoxy adhesive at various times as calculated by models with a contact interaction between the anchor and the epoxy. Again, the location of the maximum principal strain shifts from the bottom of the anchor to the top of the anchor at about 10 time units for all models. In the initial elastic step (time = 1), the maximum principal strain in the solid model with a void is about 47 percent higher than that from the corresponding solid model with no void, so the increase is larger than the 33 percent increase in the average strain that would be expected when one quarter of the epoxy is removed to create the void. At longer times, the maximum principal strains in the solid model with a void increases at a faster rate than those in the solid model without a void.

Table 2. Maximum principal strains in the epoxy for models with a contact interaction between the anchor and the epoxy.				
Time	Axisymmetric	Solid No Void	Solid With Void	
			Edge of Void	Symmetry Plane
1	1.058e-2	7.434e-3	1.090e-2	3.352e-3
10	6.192e-2	3.115e-2	6.135e-2	1.966e-2
20	1.213e-1	5.395e-2	1.014e-1	3.912e-2
50	2.439e-1	1.114e-1	2.131e-1	8.039e-2
100	3.419e-1			

Figures 17 and 18 compare the maximum principal strains as functions of time for models with a contact interaction between the anchor and the epoxy. Figure 17 plots the maximum principal strains in the thread root at the top of the anchor, and figure 18 plots the maximum principal strains in the thread root at the bottom of the anchor.

The effect of the void on the strain distribution in the epoxy is examined in figures 19 and 20, which plot the maximum principal strains in thread roots at the top and the bottom of the anchors. These figures plot the strains in thread roots at the edge of the void and the strains in the corresponding thread roots at the plane of symmetry (opposite from the void).

Figure 19 plots strains for the model with a tie constraint between the anchor and the epoxy, and figure 20 plots strains for the model with a contact interaction between the anchor and the epoxy. It can be seen from these figures that as time progresses, the strains in the model with a tie constraint become more uniform along the anchor and circumferentially, whereas the strains in the model with a contact interaction have a strong variation vertically and circumferentially. Tables 1 and 2 include columns to indicate the maximum principal strain values in thread roots adjacent to the void and in the corresponding thread root at the plane of symmetry for the models that included voids. As can be seen from Tables 1 and 2, the maximum principal strains are substantially higher at the edge of the void than at the plane of symmetry after the initial elastic step, a factor of 1.68 higher for the model with a tie constraint and a factor of 3.25 higher for the model with a contact interaction.

Contours of the  $r$ - $z$  shear strains from the models look very similar to the contours of the maximum principal strains, and their evolution over time is nearly identical. In the initial elastic step, when the epoxy responds as a glassy material, the maximum  $r$ - $z$  shear strains occur in the first or second thread roots near the free surface of the epoxy at the lower end of the anchor. Figure 21 shows contours of  $r$ - $z$  shear strains for the axisymmetric models at the end of the elastic first step. These contours can be compared to those of the maximum principal strain shown in figure 11. As the epoxy softens, the peak  $r$ - $z$  shear strain shifts from the lower end of the anchor to the top end of the anchor. For all models, this transition takes place at about 10 time units in the second (viscoelastic) step. Figure 22 shows contours of  $r$ - $z$  shear strains for the axisymmetric models after 50 time units in the second step. The locations of the shear stress concentrations in the corners of the thread roots are very similar to the locations of the maximum principal strain concentrations.

Tables 3 and 4 list the maximum calculated  $r$ - $z$  shear strains for the same conditions as in Tables 1 and 2.

Table 3. Maximum $r$ - $z$ shear strains in the epoxy for models with a tie constraint between the anchor and the epoxy.				
Time	Axisymmetric	Solid No Void	Solid With Void	
			Edge of Void	Symmetry Plane
1	1.164e-2	7.719e-3	1.062e-2	7.420e-3
10	6.083e-2	3.805e-2	4.966e-2	3.481e-2
20	1.115e-1	6.512e-2	7.657e-2	7.221e-2
50	2.548e-1	1.548e-1	1.550e-1	1.505e-1
100	4.593e-1			

Table 4. Maximum $r$ - $z$ shear strains in the epoxy for models with a contact interaction between the anchor and the epoxy.				
Time	Axisymmetric	Solid No Void	Solid With Void	
			Edge of Void	Symmetry Plane
1	1.990e-2	1.694e-2	2.023e-2	8.824e-3
10	1.113e-1	6.143e-2	1.116e-1	3.811e-2
20	2.133e-1	9.255e-2	1.963e-1	7.212e-2
50	4.329e-1	1.944e-1	4.109e-1	1.529e-1
100	6.146e-1			

Plots of the maximum  $r$ - $z$  shear strains as functions of time would look very similar to the plots of the maximum principal strains in figures 15 through 18. The shear strains are somewhat higher than the maximum principal strains, as can be seen by comparing Tables 1 through 4, so the vertical scales of the plots would differ.

Tables 3 and 4 also include columns to compare the shear strains in thread roots adjacent to the void and in the corresponding thread root at the plane of symmetry for the models that included voids. The results are similar to those already discussed for the maximum principal strains, except that the strain magnification at the edge of the void is not as large for the shear strains. Plots of the shear strains as functions of time would appear similar to figures 19 and 20.

A broad picture of the stresses in the epoxy layer will be shown using contour plots at the outer surface of the epoxy layer where it adheres to the concrete. In each of the contour plots shown in figures 23 through 34, the results from an axisymmetric model will be compared with results from the corresponding solid models with and without voids. Each figure will show the axisymmetric model on the left (with the elements swept through  $180^\circ$  to mimic the solid models), the solid model with no void in the center and the solid model with a void on the right (with the void area itself on the far right). In each figure, the upper and lower stress limits for the contours and the color for each contour will be the same for all three models shown in the figure, but the contour limits and color bands will generally be different for each figure.

Figures 23 and 24 show contours of  $r$ - $z$  shear stress  $\sigma_{rz}$  in psi and figures 25 and 26 show contours of radial normal stress ( $\sigma_{rr}$ ) in psi at the surface of the epoxy where it bonds to the concrete for the models with a tie constraint between the anchor and the epoxy. Figures 23 and 25 show contours at time step 1 and figures 24 and 26 show contours at time step 50. In all four figures, the axisymmetric model and the solid model with no void have generally similar contours. At time step 1, all models show a band of

higher shear stress near the bottom of the anchor; the void introduces an additional stress concentration in that area. At time step 1, the peak stresses in the model with the void are substantially larger (30 to 100 percent) than those for the models with no void, for both the shear stresses and the normal stresses. At time step 50, there are significant differences between the stress distributions for the model with a void and for those without. These differences arise because at time step 50, the models with no void (and perfect bonding between the anchor and the epoxy) have shifted much of the load transfer from shear through the epoxy around the circumference of the anchor to direct tension on the epoxy at the top of the anchor. The presence of the void provides freedom for the epoxy to change its volume, which reduces the development of the normal tension or compression stresses. Thus, in figure 24 at time step 50, the shear stress in the model with a void is on the order of 70 percent higher than the shear stress in the other models over most of the length of this surface. Figures 27 and 28 show contour plots of the other two normal stress components ( $\sigma_{zz}$  and  $\sigma_{\theta\theta}$ ) at time step 1 using the same contours as the plot of  $\sigma_{rr}$  in figure 25. Figures 25, 27 and 28 show very similar levels of small tensile stress over most of the anchor, with an island of compressive stress near the top of the anchor in figure 25 and 28. At time step 50, the bulk modulus of the epoxy is much larger than the shear modulus, so the epoxy behaves as a nearly incompressible material; the contour plots of the other two normal stress components ( $\sigma_{zz}$  and  $\sigma_{\theta\theta}$ ) are nearly identical to the contour plot of  $\sigma_{rr}$  at time step 50 in figure 26. In figure 26, the model with a void shows contours generally indicating a slight tensile stress, while the models without voids also show a small tensile stress over most of the surface but very large tension stresses at the top of the epoxy cylinder. The tensile stress at the top of the axisymmetric model is substantially higher than the tensile stress at the top of the solid model with no void, possibly because the axisymmetric model is more completely constrained in the tangential direction. The tie constraint between the anchor and the epoxy results in a state of triaxial tension in the epoxy over most of the length near where it bonds to the concrete, with a very high tensile stress above the anchor, which is reacting much of the force applied to the bottom of the anchor. Also, any concentration of strain or stress at the edge of the void is reduced with time, as the contours appear more nearly circumferentially uniform at longer times.

Figures 29 and 30 show contours of  $r$ - $z$  shear stress in psi and figures 31 and 32 show contours of radial normal stress ( $\sigma_{rr}$ ) in psi at the surface of the epoxy where it bonds to the concrete for the models with a contact interaction between the anchor and the epoxy. Figures 29 and 31 show contours at time step 1 and figures 30 and 32 show contours at time step 50. At time step 1, all models show higher shear stress near the bottom of the anchor; the void introduces an additional stress concentration, as shown in figure 29. At that time, the peak shear stresses in the model with the void are approximately twice as high as those for the models with no void. For these models with a contact interaction between the anchor and the epoxy, simulating only mechanical interlocking, the normal stresses over most of this epoxy/concrete interface are primarily compressive. The lack of a bond between the top of the anchor and the epoxy does not allow for load transfer to occur by tension on the top surface of the anchor, so at time step 50 in figure 30, all models show significant shear stresses. At that time, the peak shear stress in the model with a void is approximately 60 percent higher than the peak shear

stress in the models with no void. For the  $\sigma_{rr}$  normal stress contours, there are significant differences among the three models at time step 50, as shown in figure 32. All three models show a compressive stress over most of the lower 85 percent of the epoxy/concrete interface, with a transition to similar levels of tension at the top. The axisymmetric model shows a much higher compressive stress than the solid model, by about a factor of 2. This difference could be a result of the hoop direction discretization in the solid model allowing for some deformation of the epoxy that is not available in the axisymmetric model. The peak compressive stress in the solid model with a void is about twice as high as the maximum compressive stress in the axisymmetric model, but the high stress is confined to a thin region adjacent to the void. Figures 33 and 34 show contour plots of the other two normal stress components ( $\sigma_{zz}$  and  $\sigma_{\theta\theta}$ ) at time step 1 using the same contours as the plot of  $\sigma_{rr}$  in figure 31. All three of those figures show similar contours indicating compression over the lower 85 percent of the surface with tension at the top. The  $\sigma_{zz}$  and  $\sigma_{\theta\theta}$  stresses are somewhat less than the  $\sigma_{rr}$  stress at time step 1. At time step 50, the nearly incompressible behavior of the epoxy results in contours for  $\sigma_{zz}$  and  $\sigma_{\theta\theta}$  that are nearly identical to the contours for  $\sigma_{rr}$  in figure 32. The use of a contact interaction between the anchor and the epoxy results in a state of triaxial compression in the epoxy over most of the length where it bonds to the concrete. The influence of the void is not reduced with time, as the stress concentrations at the edge of the void persist.

Figures 35 through 38 show contours of the Von Mises stress on the plane of symmetry of the steel anchor. These contour plots again compare the axisymmetric model with the corresponding solid models. The void in these figures is to the left of the anchor. The upper and lower limits and the color for each contour are the same for all four of these figures. Figures 35 and 36 plot contours of the Von Mises stress in the anchor for models with a tie constraint between the anchor and the epoxy at time step 1 and time step 50. Figures 37 and 38 plot contours of the Von Mises stress in the anchor for models with a contact interaction between the anchor and the epoxy at time step 1 and time step 50. For each case shown, the results from the solid model with no void generally match to the results from the axisymmetric model. Also, the results at time step 1 are very similar for the two types of interface between the anchor and the epoxy. At time step 50, for cases with a tie constraint between the anchor and the epoxy, both the axisymmetric model and the solid model with no void had stresses at the top of the anchor that are much higher than for the other cases, corresponding to the transition to a situation where more of the anchor loading is reacted by a direct tension at the top of the anchor. The contour plots indicate that the maximum Von Mises stress in the anchors of the axisymmetric models is much higher than in the solid models. These peak stresses occur in the thread roots of the anchor, and are better captured by the finer mesh of the axisymmetric models.

Figures 39 through 42 plot contours of the maximum principal stress at the plane of symmetry and within the hole in the concrete, again comparing the axisymmetric models with the corresponding solid models. In each figure, the axisymmetric model is to the left; the solid model with no void is in the center and the solid model with the void is to the right. The void itself is along the left hand side of the hole.

Figure 39 shows the models with a tie constraint between the anchor and the epoxy at time step 1. All three models have a stress concentration near the bottom at the free edge of the epoxy. The solid model with a void has asymmetric contours and a peak stress of approximately 20 to 30 percent higher than the peak stress for the other two models. Figure 40 shows the models with a tie constraint between the anchor and the epoxy at time step 50. The maximum principal tensile stresses in the axisymmetric model and the solid model with no void are very high and occur at the top of the hole in the concrete, reflecting the change in the load transfer mechanism from shear through the epoxy around the circumference of the anchor to direct tension through the epoxy at the top end of the anchor.

Figure 41 shows the models with a contact interaction between the anchor and the epoxy at time step 1. The solid model with a void has asymmetric contours and a peak stress of approximately 30 to 50 percent higher than the peak stress for the other two models. Figure 42 shows the models with a contact interaction between the anchor and the epoxy at time step 50. At that time, the axisymmetric model shows very high levels of maximum principal stress, which is primarily tensile hoop stress developed in response to the large compressive stress introduced by the epoxy at the interface. The solid model with a void has locally high stress levels of similar magnitude, which appear to be related to hoop stress in response to locally high compressive stresses in the epoxy at the edge of the void and a locally high tensile stress in the epoxy at about the top of the anchor.

## Summary

The anchor geometry has two discontinuities that result in stress concentrations. One is near the bottom of the anchor at the point where the epoxy adhesive layer terminates, and one is at the top end of the anchor itself. Initially, when the epoxy reacts as a glassy material, the stresses and strains are highest near the bottom of the anchor, with most of the applied load reacted within the first 1 to 2 inches from the edge of the epoxy layer, judging by the decay in anchor stress and average shear stress in the contour plots. As time increases, and the epoxy softens, the highest stresses and strains shift to the epoxy at the top thread of the anchor. For all the models, the transition occurred at about 10 time units in the second viscoelastic step, and the general shape of the distribution of stresses and strains did not change significantly thereafter.

In addition to shear stresses, the anchor system also develops normal stresses within the epoxy adhesive layer. In general, the radial, tangential and vertical normal stresses are of the same sign and similar magnitude, especially at longer times when the epoxy behavior is becoming more incompressible. For models with a tie constraint between anchor and epoxy (simulating perfect bonding), the normal stresses are predominantly tensile, and at long times, the perfect bonding leads to large tensile stresses at the top of the anchor to react the force applied at the bottom of the anchor. For the models with a contact interaction between the anchor and the epoxy to simulate only a mechanical interlock, the normal stresses are predominantly compressive.

Assuming that the initial elastic response can be extrapolated to higher loads, a prediction of the relative pullout strength for models with and without voids could be made. Anchor pullout can involve fracture in both the concrete and the epoxy. Assuming that the epoxy and concrete behave as brittle materials, a critical value of the maximum principal strain or stress could be used to predict fracture initiation. In the initial elastic step, for models with a tie constraint between the anchor and the epoxy, the maximum principal strain in the epoxy was about 42 percent higher and the maximum principal stress in the concrete was about 33 percent higher in the model with a void than in the model without. In the initial elastic step, for models with a contact interaction between the anchor and the epoxy, the maximum principal strain in the epoxy was about 47 percent higher and the maximum principal stress in the concrete was about 50 percent higher in the model with a void than in the model without. In both cases, the increase is as large or larger than the expected 33 percent increase in the average stress or strain resulting from a removal of 25 percent of the epoxy from the anchor.

The two types of interaction studied led to different maximum principal strain concentrations in the epoxy in the thread roots. For models with a tie constraint between anchor and epoxy, there were two strain concentrations at the top and bottom corner of each thread root, with the strain concentration at the top corner being slightly larger. For models with a contact interaction between anchor and epoxy, there was a single strain concentration at the bottom surface of the thread root near to the corner. Both horizontal cracks emanating from the top corner of a thread root and slanted cracks emanating from the bottom of a thread root near the corner were observed in the epoxy from a cored anchor (see figure 21 in Materials Laboratory Factual Report 06-073). This result could indicate a mix of interaction conditions or a sequence where one type of fracture precedes and leads to the other.

All of the anchors from the accident location separated cleanly from the epoxy at the top surface of the anchor (see Materials Laboratory Factual report 06-091), suggesting that the bond between the anchor and epoxy is weak in direct tension. When removing epoxy from the anchors for testing, it separated cleanly under negligible force in some cases, but in other cases required a good deal of force. A wide variety of possible interaction conditions between the anchor and the epoxy could be considered; the tie constraint and the frictionless contact interaction were intended to examine the outer bounds of the possible interactions.

Some of the results in the model with a void and a contact interaction between the anchor and the epoxy could be affected by the (small) horizontal motion of anchor, as the anchor slips toward the void, increasing the lever arm for any bending of the epoxy thread profile. If the helical thread geometry had been included, the anchor might have been required to rotate about its own axis as well as translate in order to move into the void.

The helical geometry of the threads was neglected so as to be able to compare the solid models with the axisymmetric models directly, as well to make use of mirror symmetry and to simplify the geometry description and mesh generation. The slope of the threads is

only about 5 percent, and this feature of the geometry was considered as not significant compared to the thread profile. The void model is also simplified; examination of void areas on anchors from the tunnel showed that the epoxy generally wetted both the anchor and the hole leading to a void with a smooth boundary.

A relatively coarse mesh was found to be necessary for the solid models with a contact interaction between the anchor and the epoxy, as models with a more refined mesh had difficulty converging to a solution. The coarse mesh appeared adequate to capture the overall features of the problem for models with a tie constraint between anchor and epoxy, as shown by the good agreement between the solid model with no void and the axisymmetric model for the anchor displacements and stresses at the epoxy/concrete interface. For the solid models with contact, it appeared that the coarse mesh allowed some interpenetration in the solid model that was not observed in the axisymmetric model; a different choice of options in specifying the contact interaction might improve the behavior. In general, the strains calculated in the solid model were about half as large as those calculated in the axisymmetric model.

It was planned to use the results of these relatively coarse solid models as a basis for submodels focused on areas of stress or strain concentrations. Time constraints require that any investigations using submodels be deferred. Submodeling might not work anyway in the contact case, if there is excessive interpenetration in the coarse model, the boundary conditions imposed on the submodel would be incorrect. Because of the large variations in material properties, the deformation is not confined, so the mesh must be similarly refined along the length of the anchor. Also, the contact interaction used requires similar mesh density for the anchor and the epoxy.

Although the calculated anchor displacement is not large, the calculated strains in the epoxy are substantial, suggesting that fracture or yielding of the epoxy might occur. (The models did not allow for fracture or yielding of the epoxy.) Although epoxies are generally considered to be brittle materials, they can exhibit yield behavior. Unlike metals, yield in polymers does generally depend on the hydrostatic stress [5].

At longer times, both types of models lead to interesting results with respect to the stresses in the concrete. For the axisymmetric and solid model with no void and a tie constraint between the anchor and the epoxy, the perfect bonding leads to the applied load being reacted by direct tension at the top of the anchor. The resulting tensile stress in the concrete probably exceeds its tensile strength. It should be noted, however, that nearly all of the anchors from the tunnel had a clean separation between the top of the anchor and the epoxy above the anchor, even for anchors with modest downward displacement, indicating that the bond between the anchor and the epoxy would fracture before stresses in the concrete above the anchor reached a critical level. For the axisymmetric model with a contact interaction between the anchor and the epoxy, the triaxial compressive stress developed in the epoxy leads to significant hoop stresses in the concrete.

With a constant bulk modulus, the decrease in the shear modulus makes the epoxy behave more like an incompressible material (in which case Poisson's ratio approaches

0.5). The inorganic fillers in the epoxy should have a much stronger effect on the epoxy bulk modulus than on its shear modulus, so the epoxy might start out as a nearly incompressible material. Because of the uncertainty in the properties of the epoxy, models were also run with an initial epoxy Poisson's ratio of 0.49, and the results from those calculations were similar to the results reported herein (using an initial epoxy Poisson's ratio of 0.3).

Carl R. Schultheisz  
Materials Research Engineer

## References

1. E. Oberg, F.D. Jones, H.L. Horton and H.H. Ryffell, Machinery's Handbook, 26<sup>th</sup> Edition, Industrial Press, Inc., New York, 2000.
2. G. Winter and A.H. Nilson, Design of Concrete Structures, Eighth Edition, McGraw-Hill Book Company, New York, 1972.
3. A.S. Wineman and K.R. Rajagopal, Mechanical Response of Polymers, Cambridge University Press, Cambridge, 2000.
4. J.D. Ferry, Viscoelastic Properties of Polymers, John Wiley and Sons, New York, 1961.
5. I.M. Ward, Mechanical Properties of Solid Polymers, Second Edition, John Wiley and Sons, Chichester, 1983.

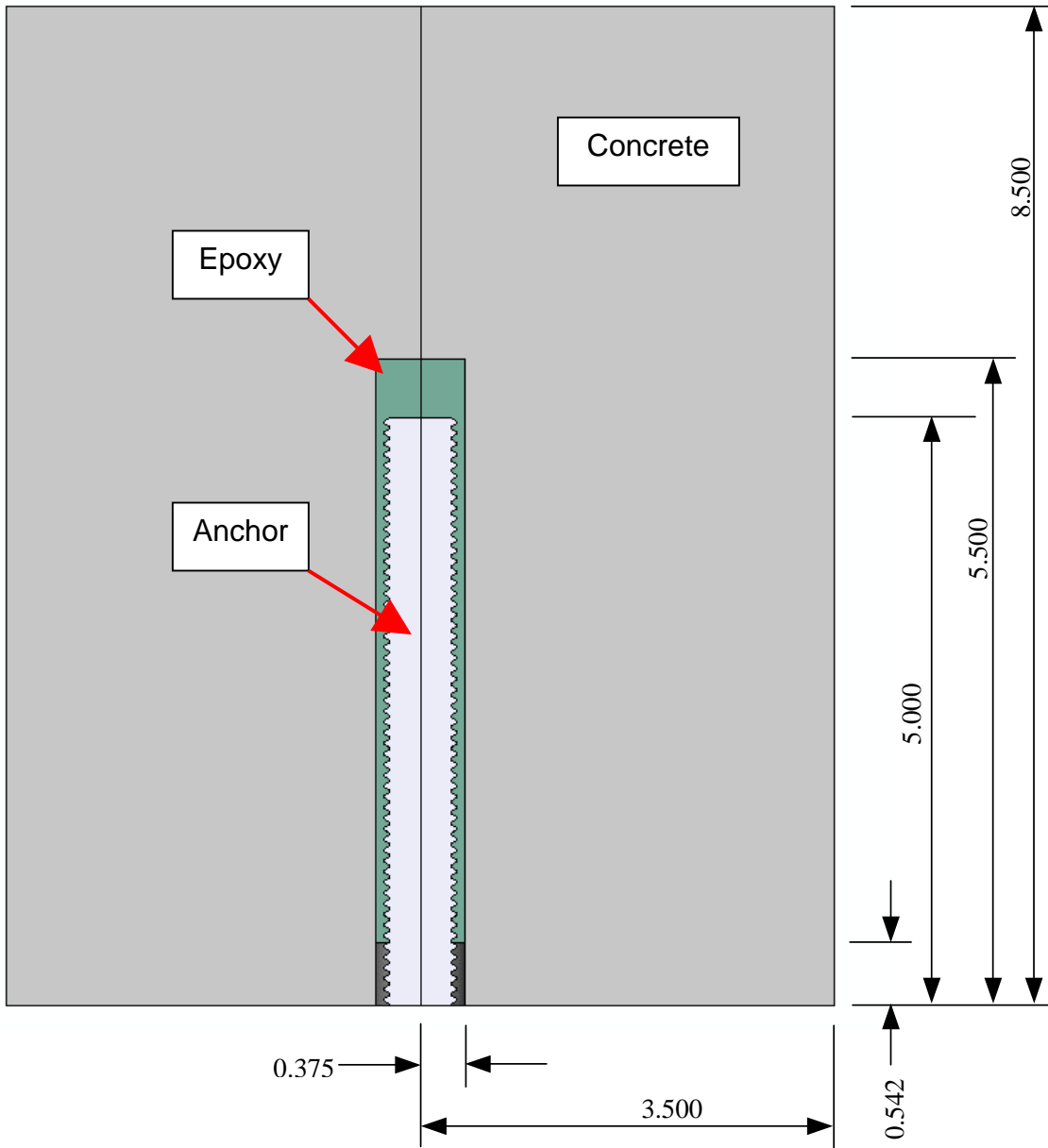


Figure 1. Geometry of the models investigated. Dimensions indicated are in inches.

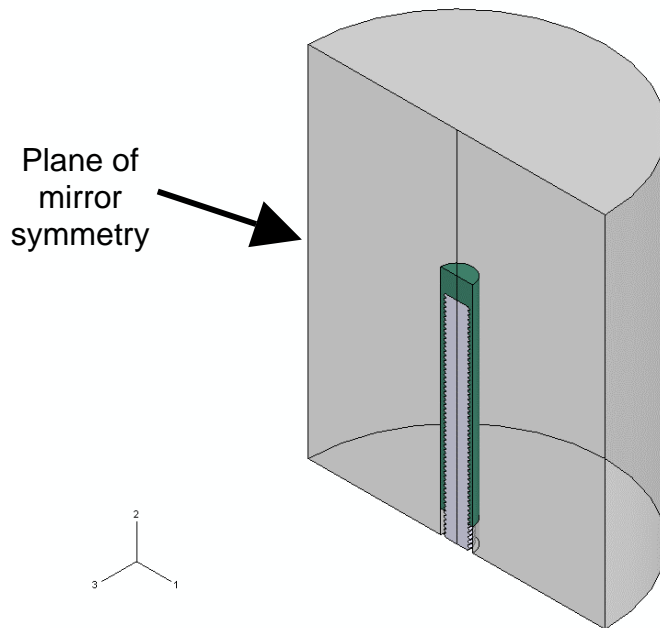


Figure 2. Oblique view showing the geometry of the anchor, the epoxy adhesive layer and the outer concrete cylinder used in the models. The plane through the center of the anchor, epoxy and concrete was used as a plane of symmetry to reduce the size of the problem.

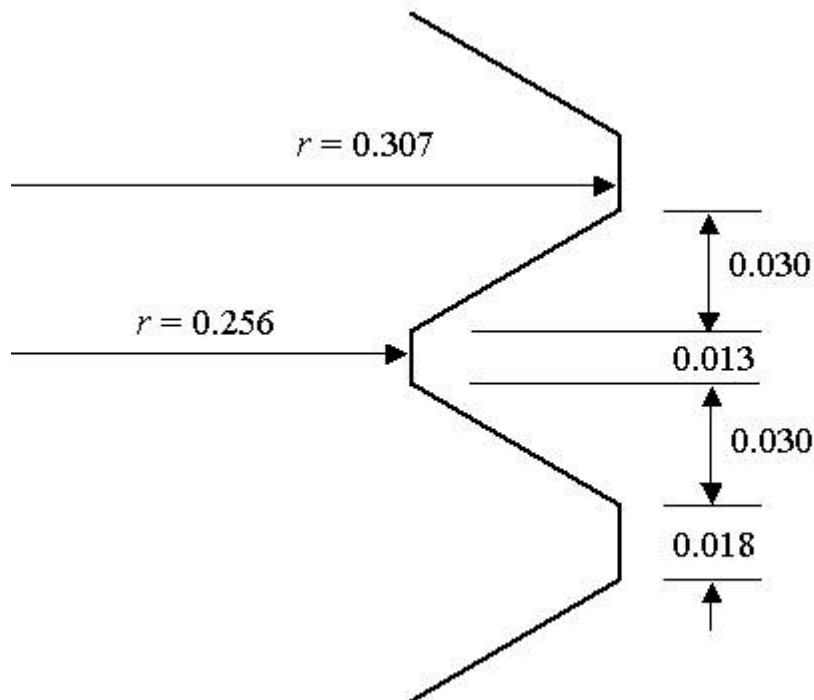


Figure 3. Thread profile used for the anchor in the models. For the axisymmetric models, this profile was modified to include a 0.002-inch radius on all corners (interior and exterior). Dimensions indicated are in inches.

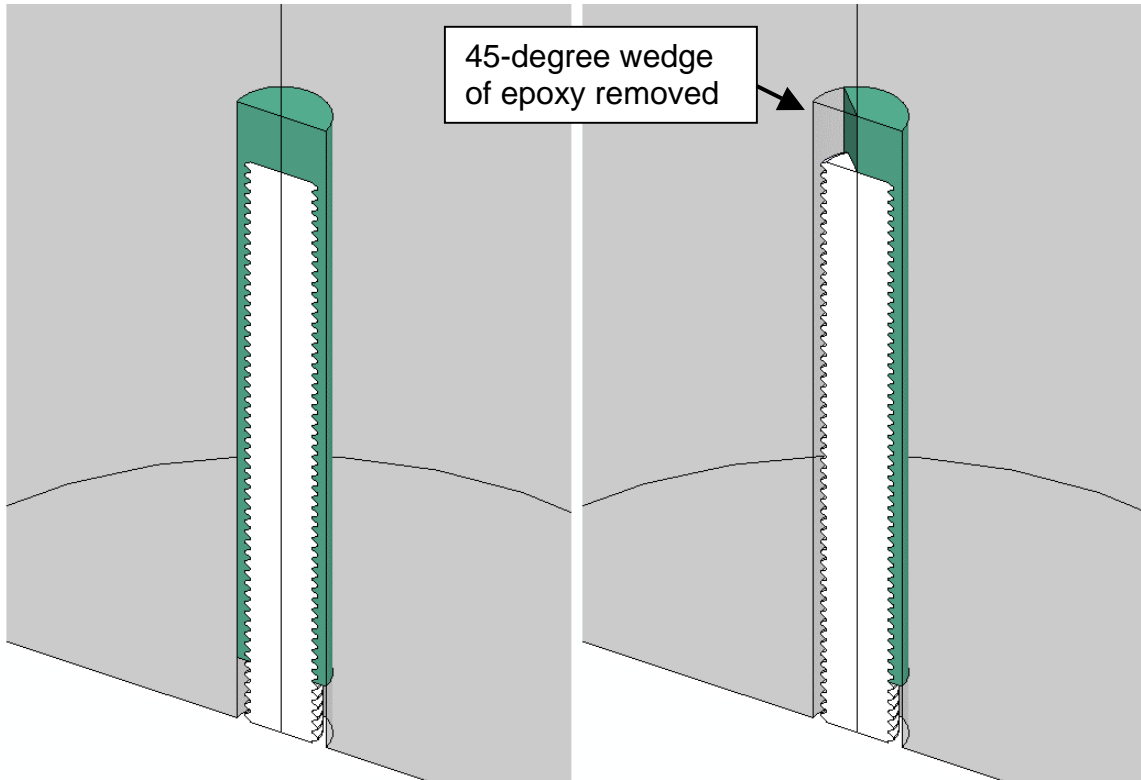


Figure 4. Oblique cutaway views showing the geometry of the epoxy without a void on the left and with a void on the right.

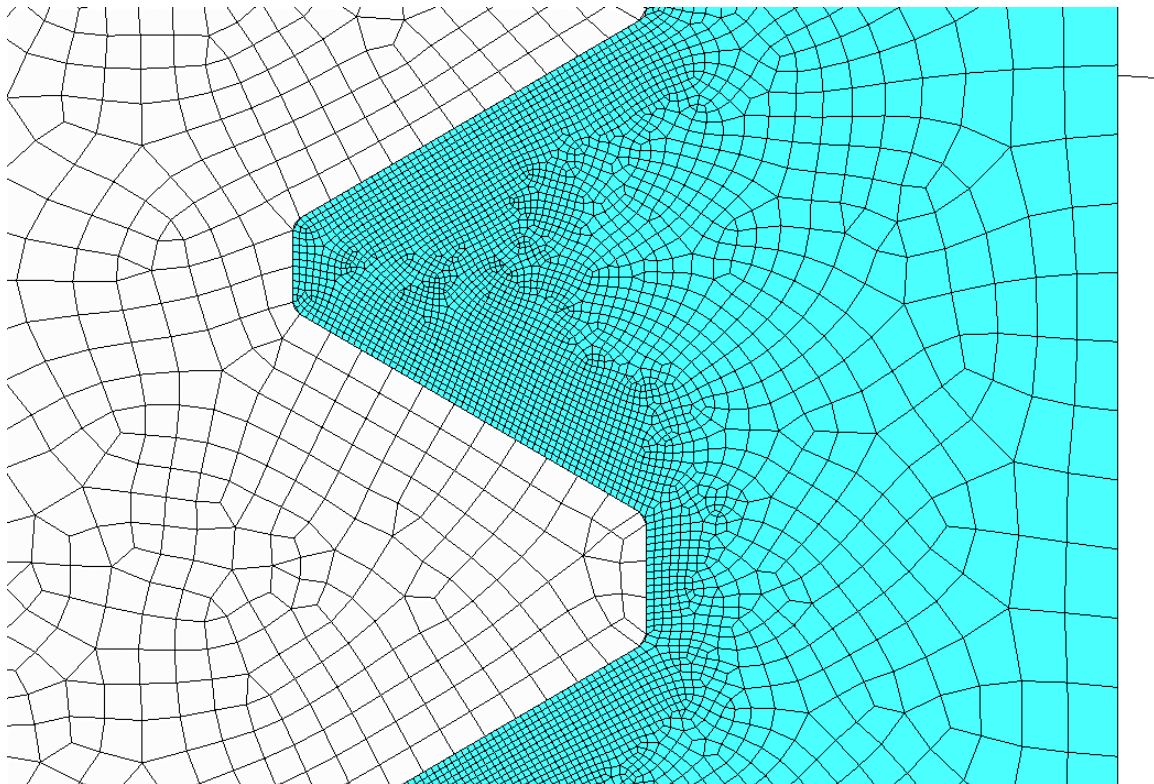


Figure 5. Representative view of the mesh used for the axisymmetric models. Anchor to the left in white; the full thickness of the epoxy adhesive layer in blue.

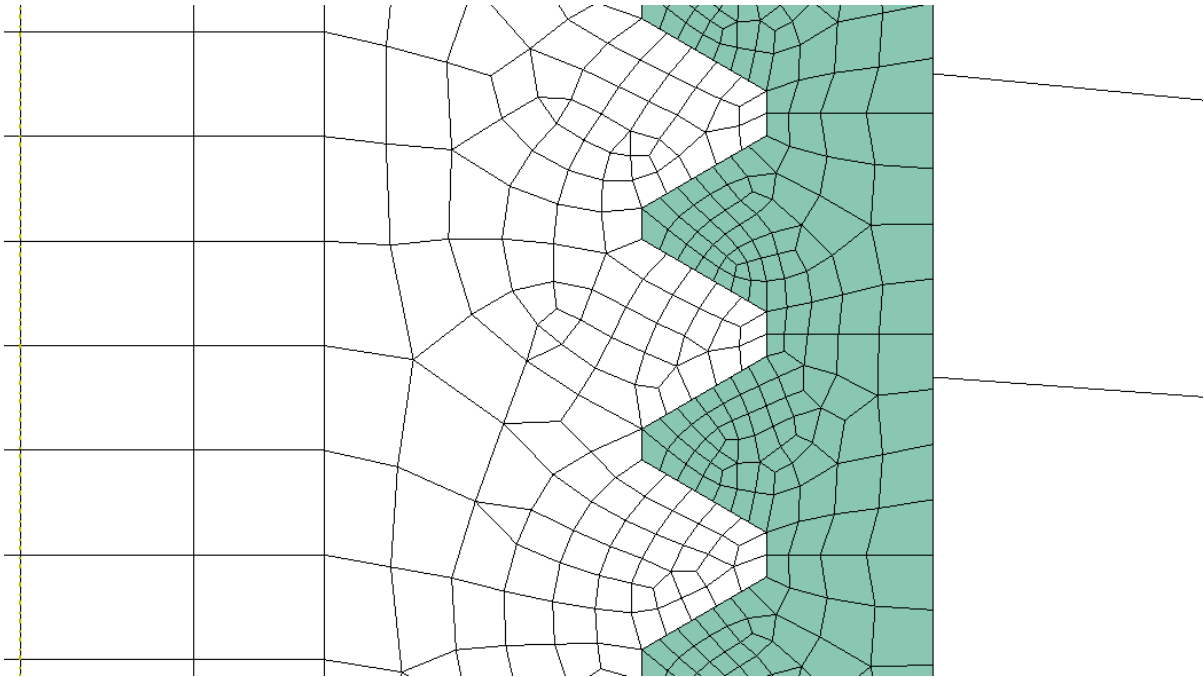


Figure 6. Representative view of the mesh used for the solid models. Anchor to the left in white (dashed centerline of the anchor just at the edge of the image); epoxy adhesive in green and concrete cylinder in white to the right.

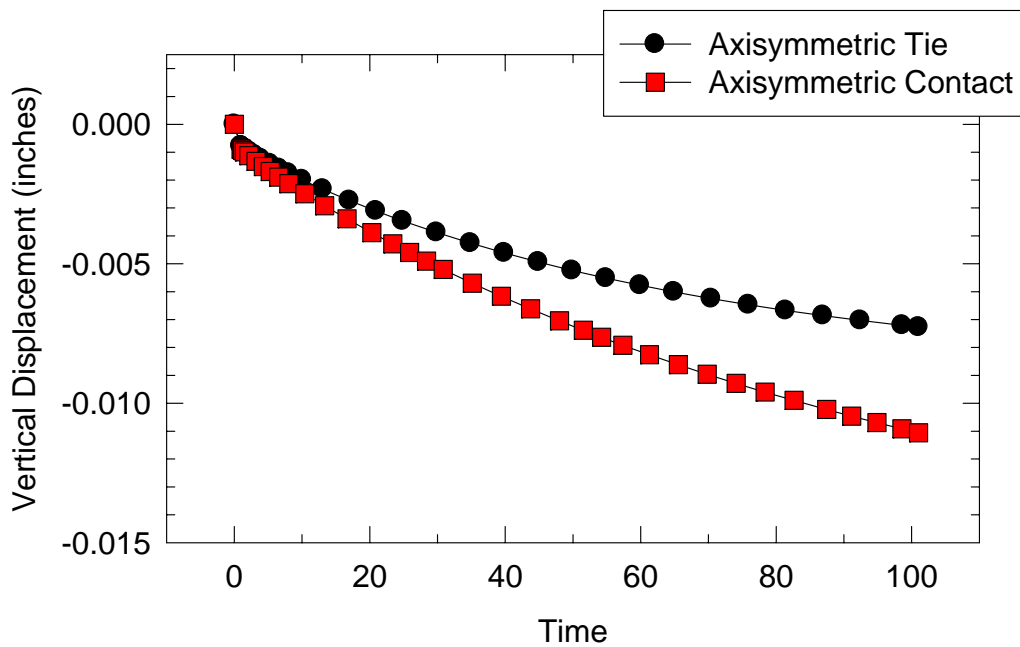


Figure 7. Vertical displacement of the bottom end of the anchor as calculated using the two dimensional axisymmetric models.

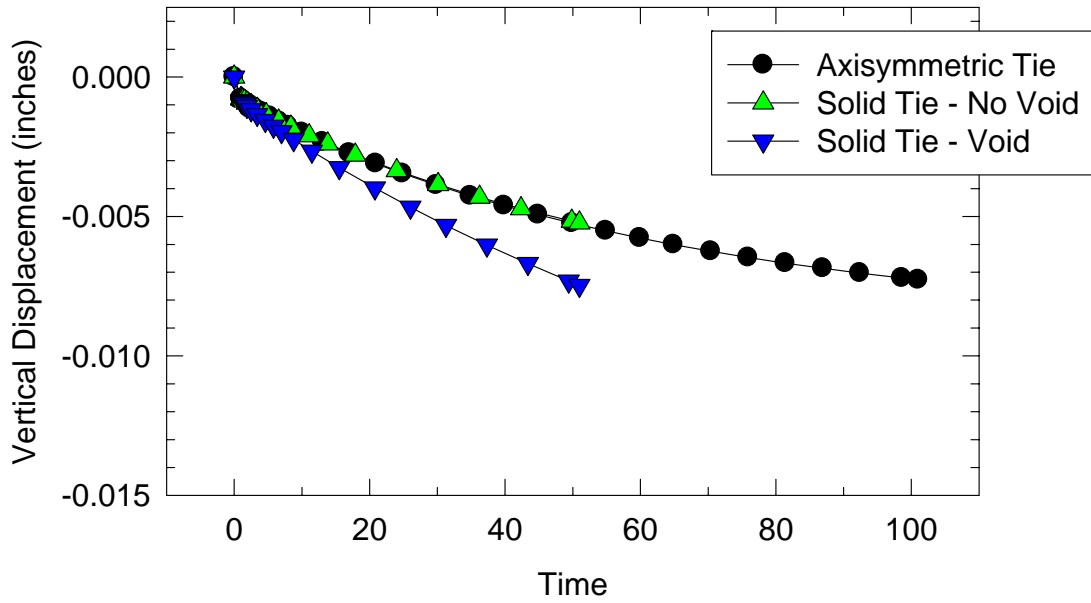


Figure 8. Vertical displacement of the bottom end of the anchor calculated using the models with a tie constraint (perfect bonding) between the anchor and the epoxy. The results from the solid model with no void are similar to the results of the axisymmetric model.

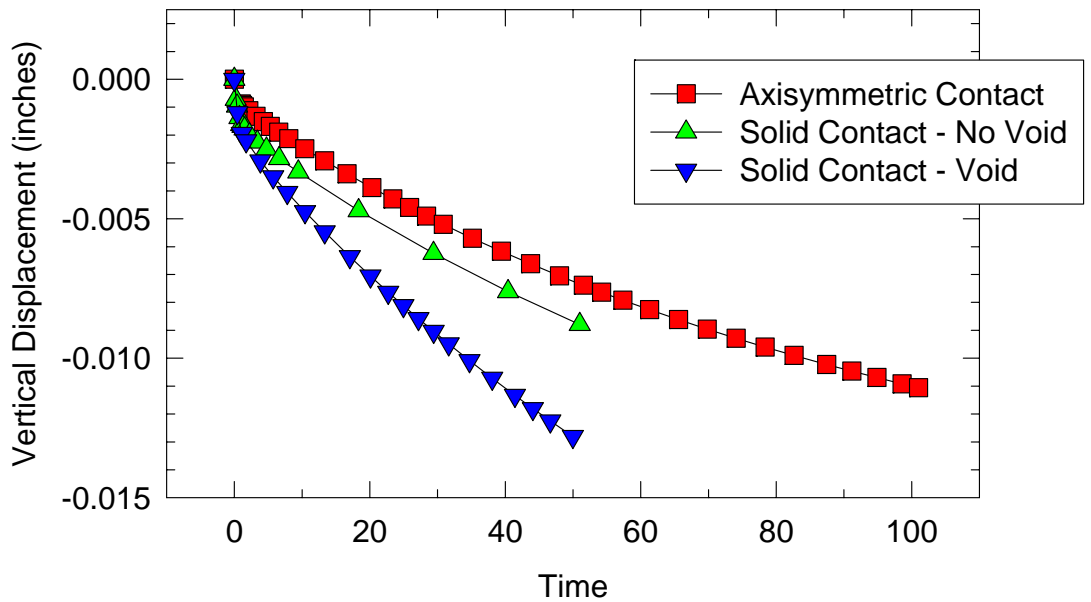


Figure 9. Vertical displacement of the bottom end of the anchor calculated using the models with a contact interaction (mechanical interlocking only) between the anchor and the epoxy.

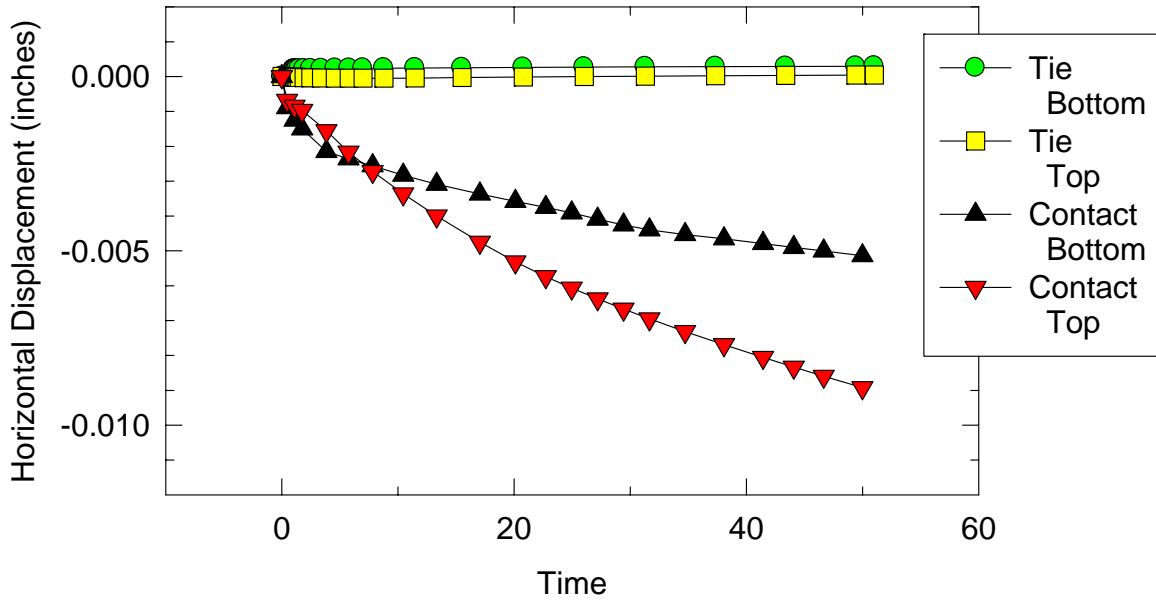


Figure 10. Horizontal displacement of the top and bottom ends of the anchor for the solid models with voids. Positive displacement is away from the void, negative displacement toward the void. The anchor with a tie constraint shifts slightly away from the void. For the model with the contact interaction, the bottom of the anchor begins to slide toward the void first, followed by the top of the anchor.

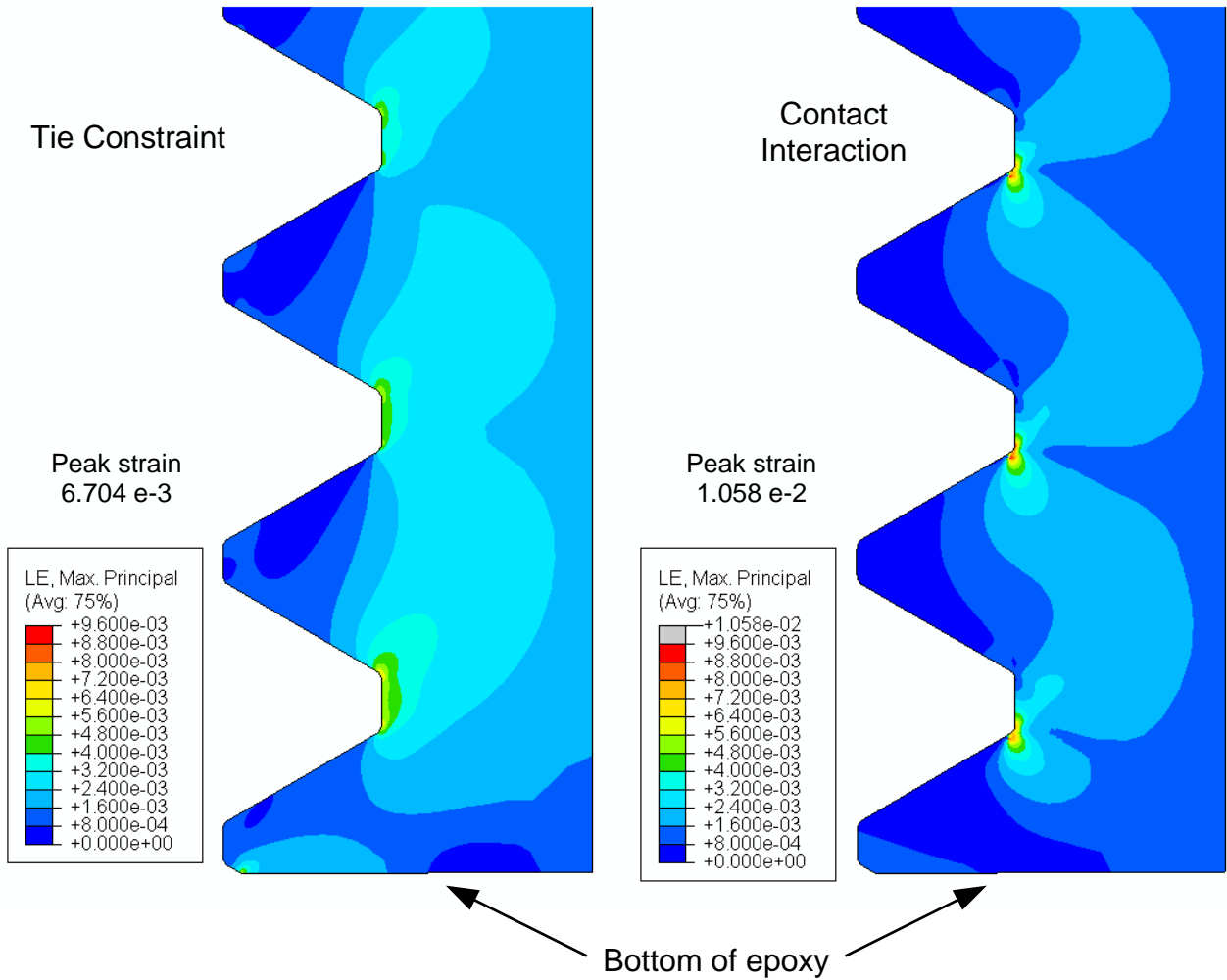


Figure 11. Contours of maximum principal strain showing the strain concentrations in the thread roots of the epoxy layer near the bottom of the anchor. These images are from the axisymmetric models at the end of the elastic step. The model with a tie constraint between the anchor and the epoxy is on the left, and the model with a contact interaction between the anchor and the epoxy is on the right. The anchor and concrete were suppressed for these images. The tie constraint leads to two strain concentrations at the top and bottom of each thread root, with the strain concentration at the top of the thread root being slightly larger. The contact interaction creates a sharper strain concentration at the bottom corner of each thread root.

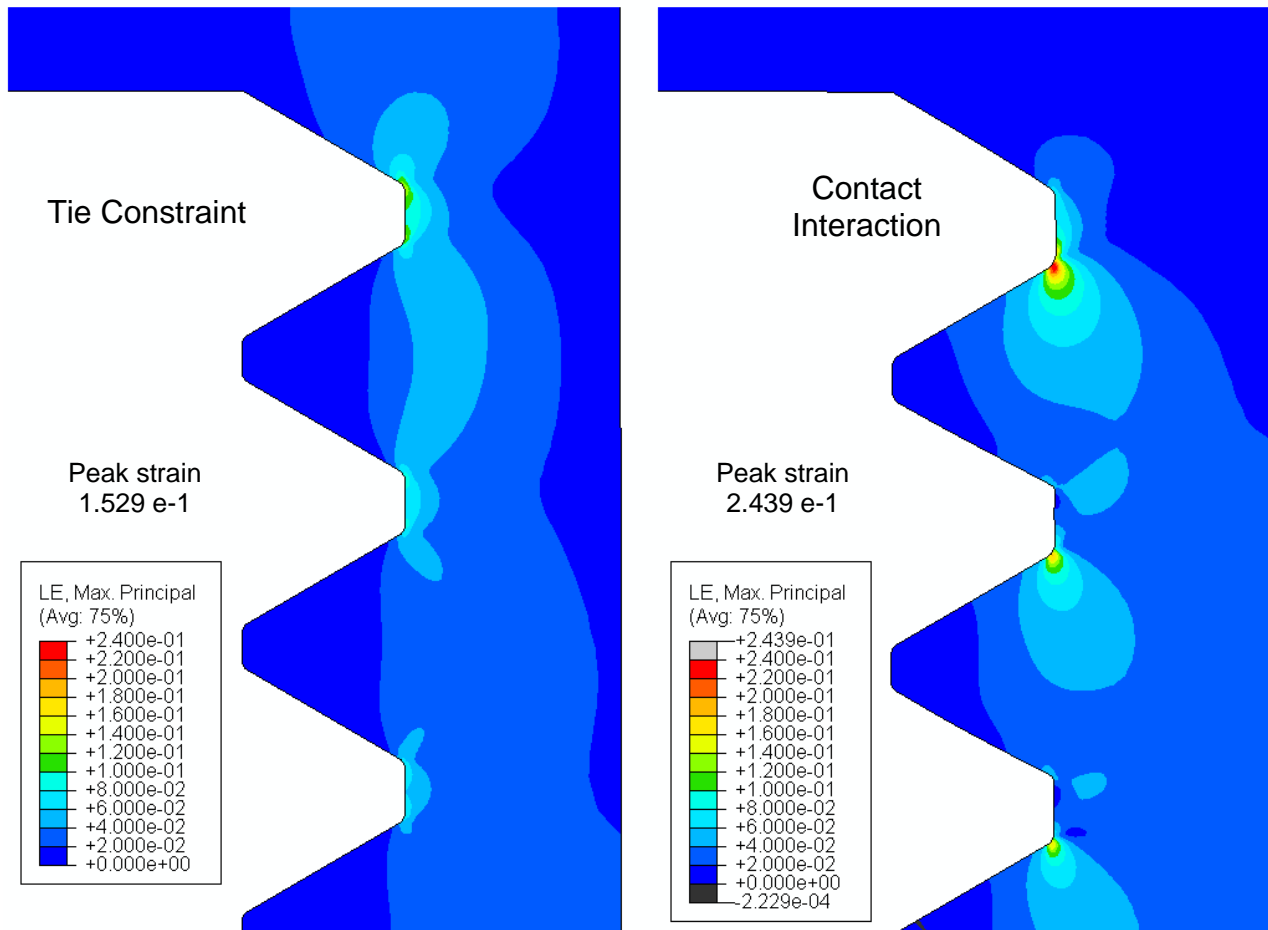


Figure 12. Contours of maximum principal strain in the epoxy layer at the top of the anchor from the axisymmetric models after 50 time units of the second (viscoelastic) step. Tie constraint on the left, contact interaction on the right. The anchor and concrete were suppressed in the images. The locations of the strain concentrations in the thread roots are similar to those in figure 11. Note the significant deformation in the top thread root in the model with contact on the right.

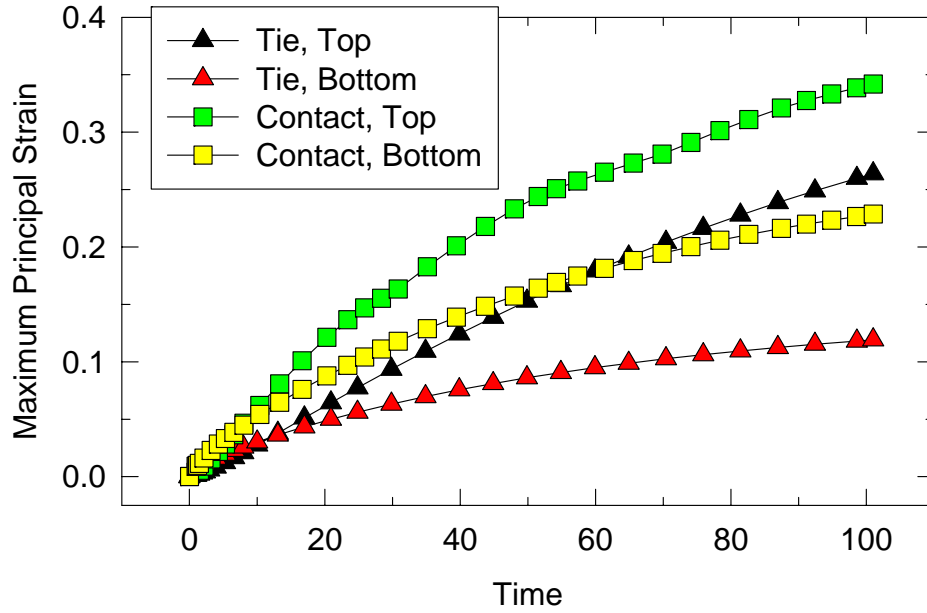


Figure 13. Peak values of the maximum principle strains in the epoxy layer from the axisymmetric models as a function of time. At long times, the peak strains shift from the thread roots at the bottom of the anchor to the thread roots at the top of the anchor.

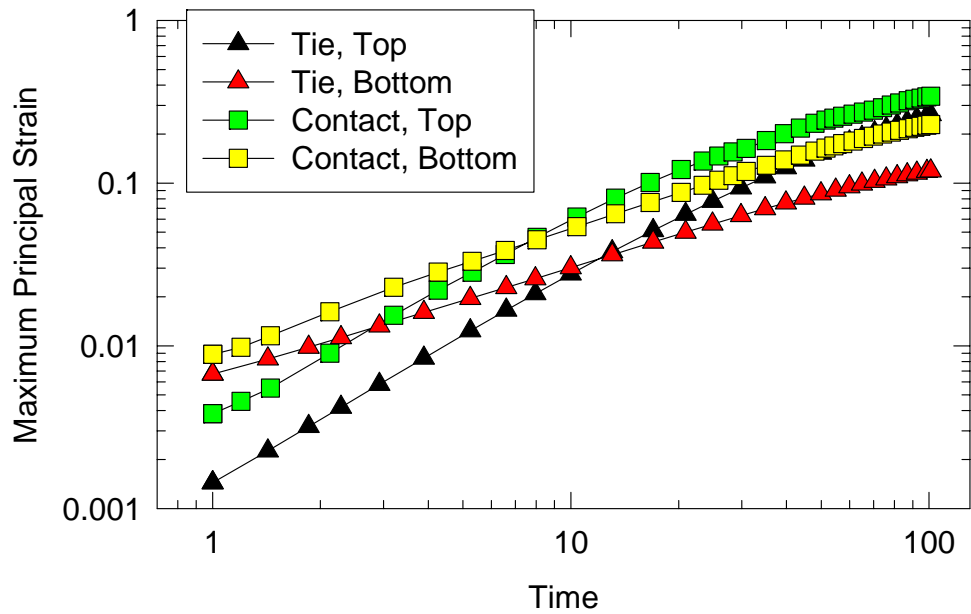


Figure 14. The same data as that shown in Figure 13, but on logarithmic scales, showing the transition in the location of the peak strains from the bottom thread roots at short times (elastic response) to the top thread roots at longer times. The transition occurred at approximately 10 time units for all models.

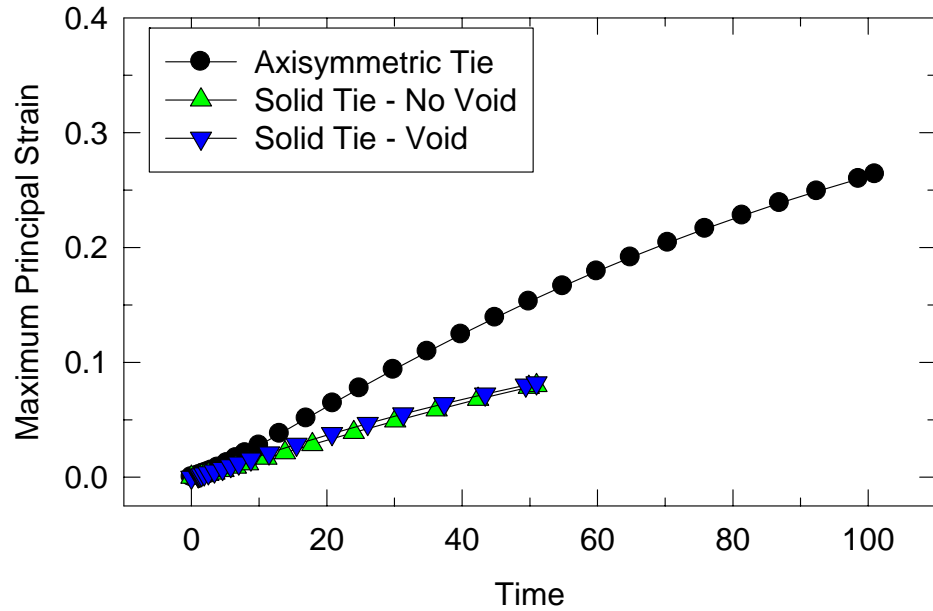


Figure 15. Peak values of the maximum principal strains in the epoxy in the thread root at the top of the anchor, as calculated from models with a tie constraint between the anchor and the epoxy. At long times, the peak strains at this location for the models with and without voids become very similar.

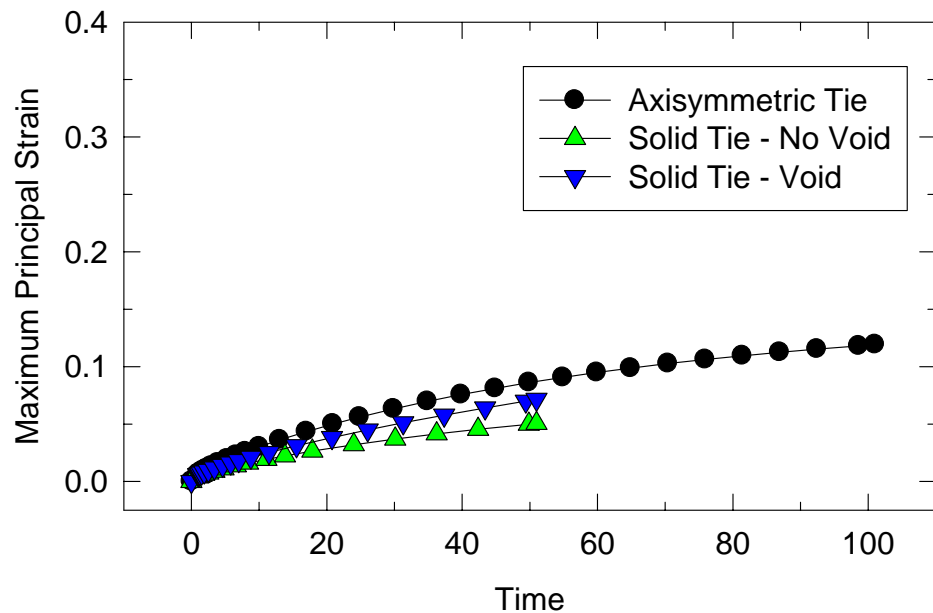


Figure 16. Peak values of the maximum principal strains in the epoxy in the thread root at the bottom of the anchor, as calculated from models with a tie constraint between the anchor and the epoxy. Initially, these peak strains are larger than those at the top of the anchor (above). Peak strains at the top and bottom of the anchor are more similar for the solid model with a void than for the other two models.

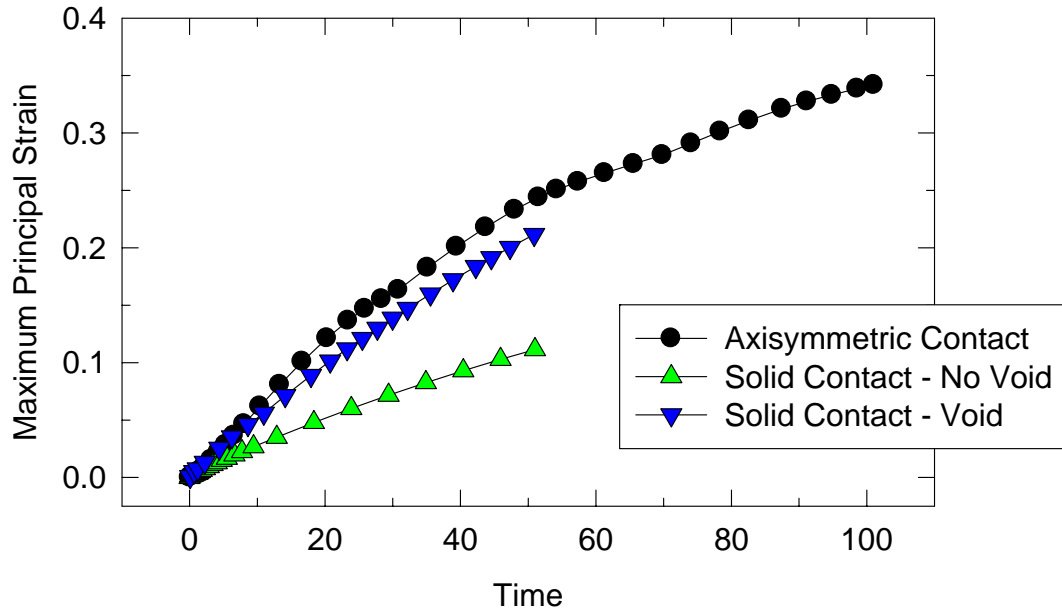


Figure 17. Peak values of the maximum principal strains in the epoxy in the thread root at the top of the anchor, as calculated from models with a contact interaction between the anchor and the epoxy.

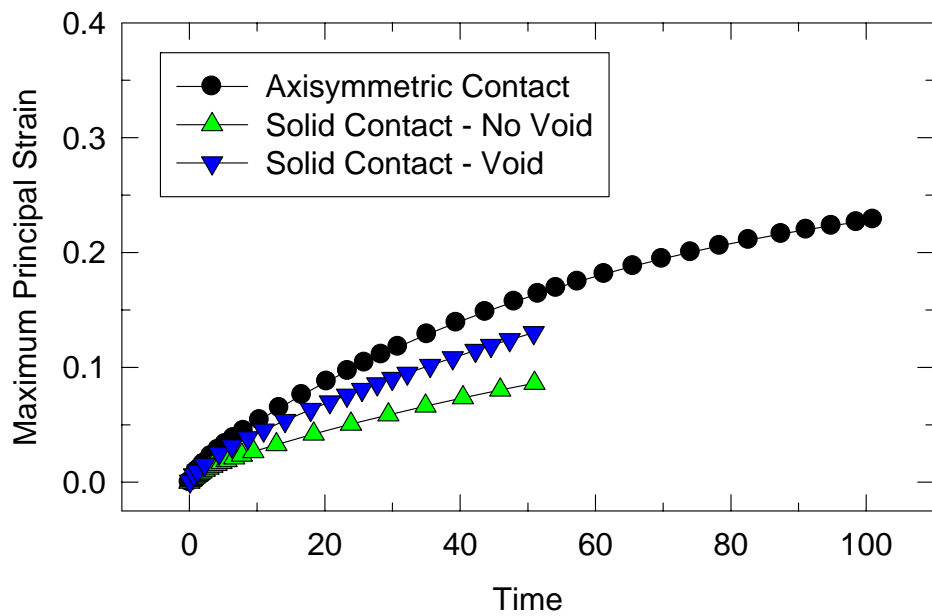


Figure 18. Peak values of the maximum principal strains in the epoxy in the thread root at the bottom of the anchor, as calculated from models with a contact interaction between the anchor and the epoxy. Initially, these peak strains are larger than those at the top of the anchor (above).

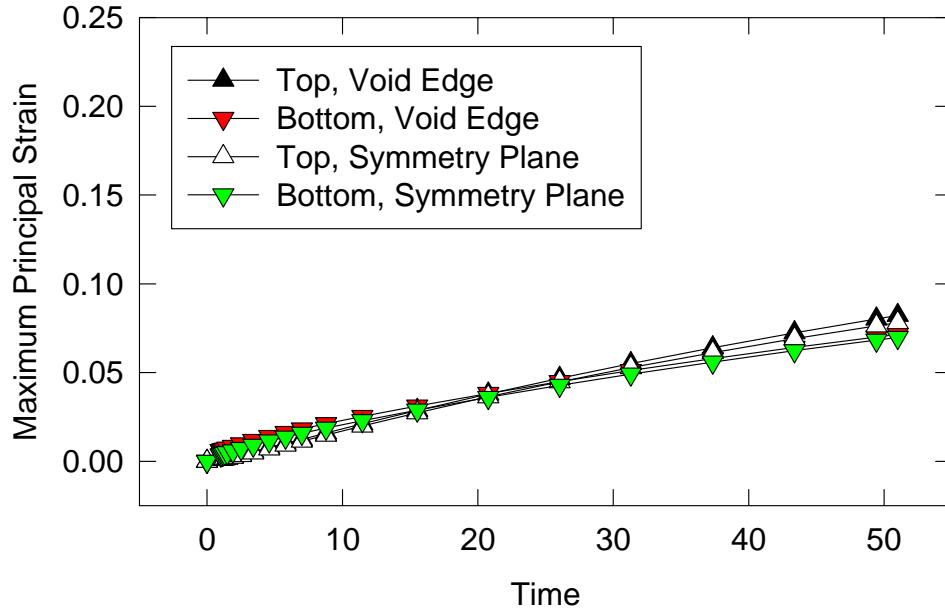


Figure 19. Comparison of the peak values of the maximum principal strains in the epoxy at the edge of the void and at the plane of symmetry for models with a tie constraint between the anchor and the epoxy. These data are from thread roots at the top and bottom of the anchor.

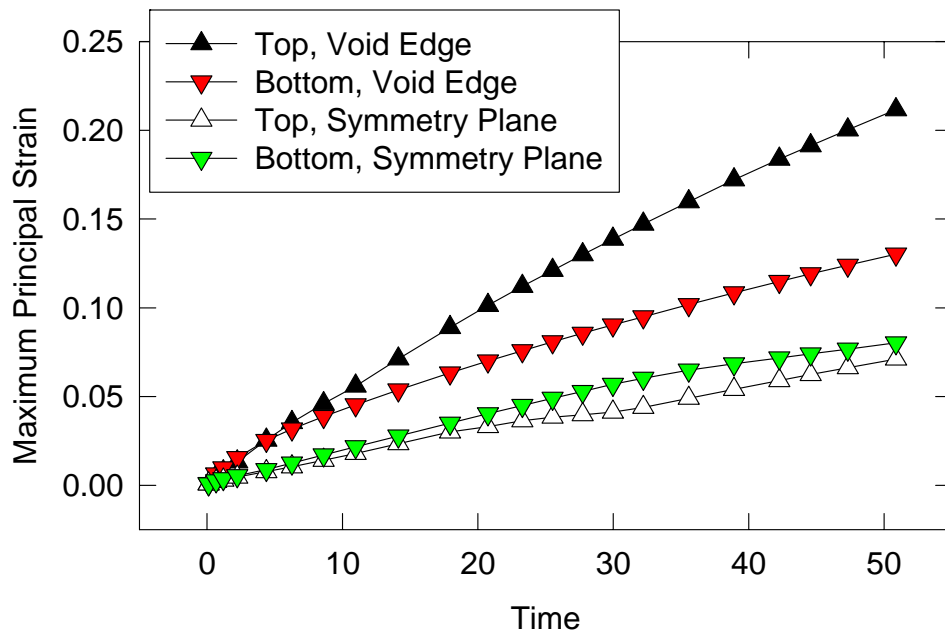


Figure 20. Comparison of the peak values of the maximum principal strains in the epoxy at the edge of the void and at the plane of symmetry for models with a contact interaction between the anchor and the epoxy. These data are from thread roots at the top and bottom of the anchor.

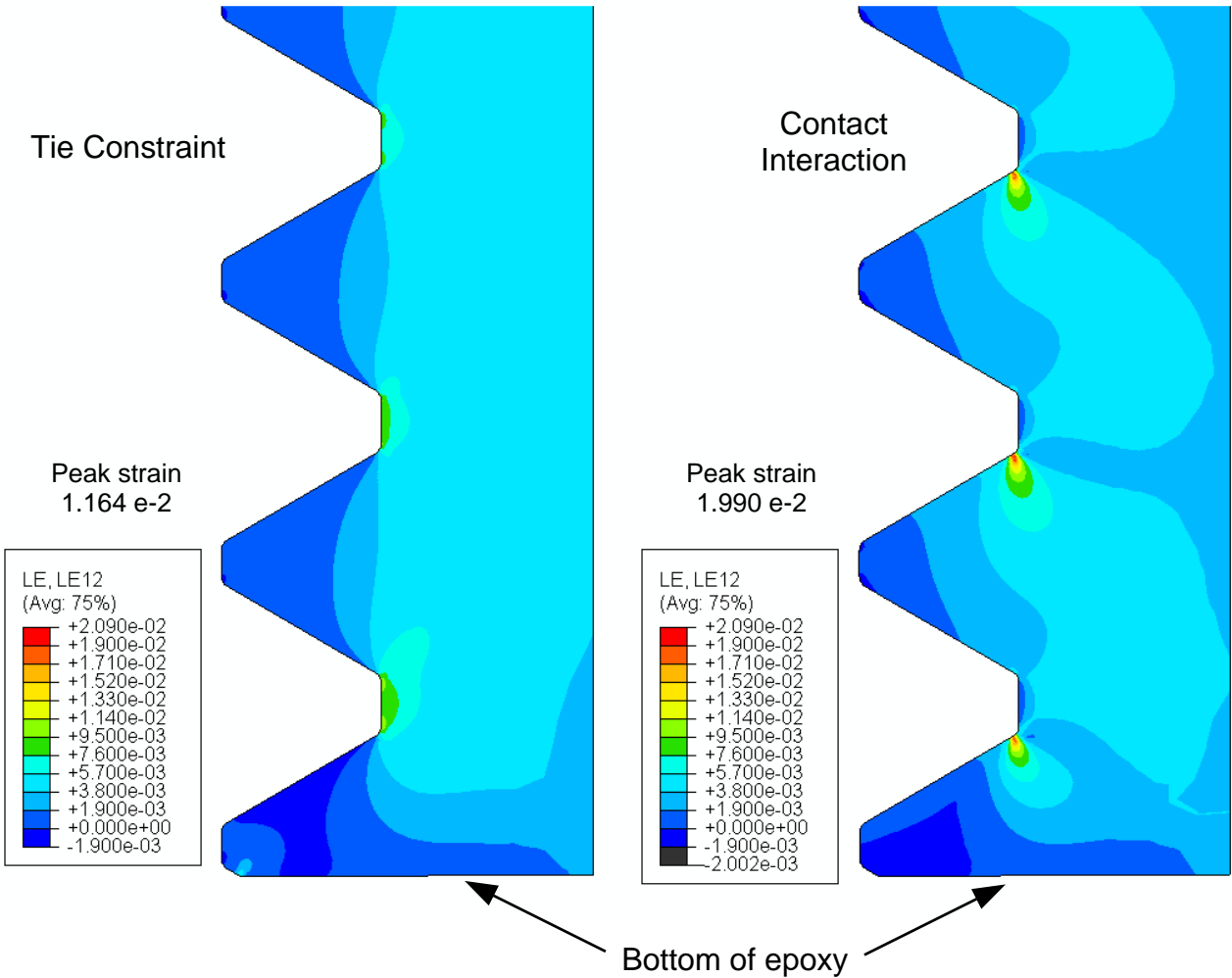


Figure 21. Contours of  $r$ - $z$  shear strain (directions 1 and 2 in the models) in the epoxy layer near the bottom of the anchor from the axisymmetric models at the end of the elastic step. These contours are generally similar to those of the maximum principal strain in figure 11. The tie constraint on the left leads to two nearly symmetric shear strain concentrations at the top and bottom of each thread root. The contact interaction on the right creates a sharper strain concentration at the bottom corner of each thread root.

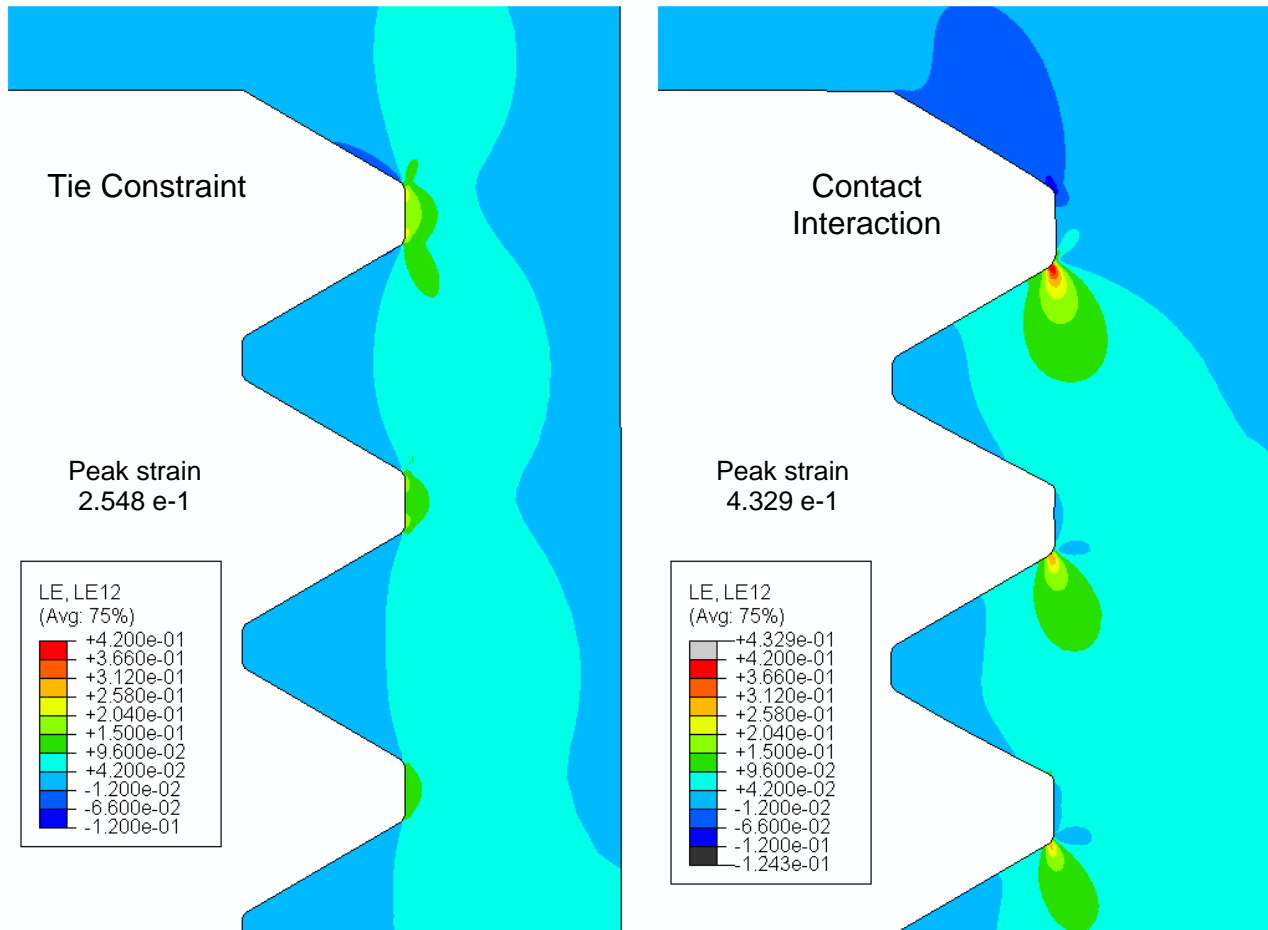


Figure 22. Contours of  $r$ - $z$  shear strain (directions 1 and 2 in the models) in the epoxy layer at the top of the anchor from the axisymmetric models after 50 time units of the second (viscoelastic) step. Tie constraint on the left, contact interaction on the right. The strain contours are generally similar to those for the maximum principal strain shown in figure 12. Note significant deformation in top thread root in the model with contact on the right.

Tie Constraint

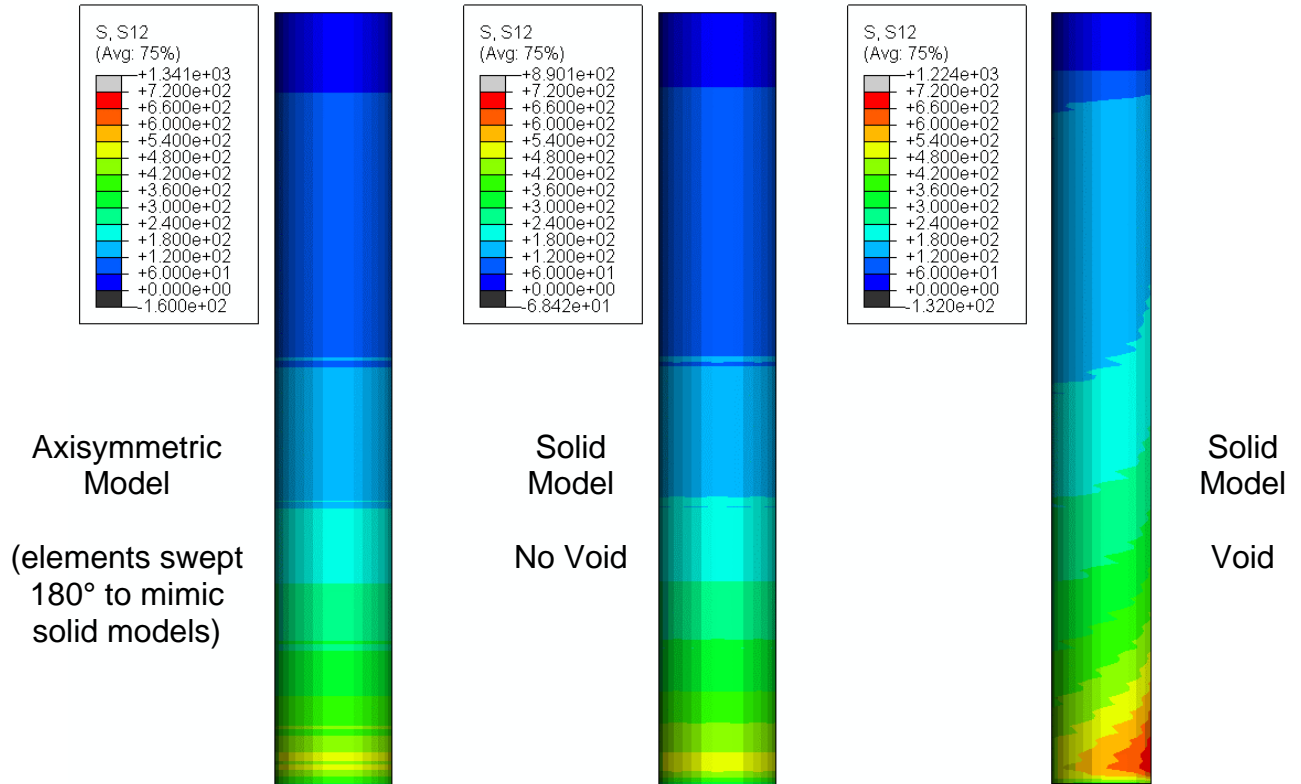


Figure 23. Contours of  $r$ - $z$  shear stress (in psi) at time step 1 at the epoxy surface where it bonds to the concrete, for models with a tie constraint between anchor and epoxy.

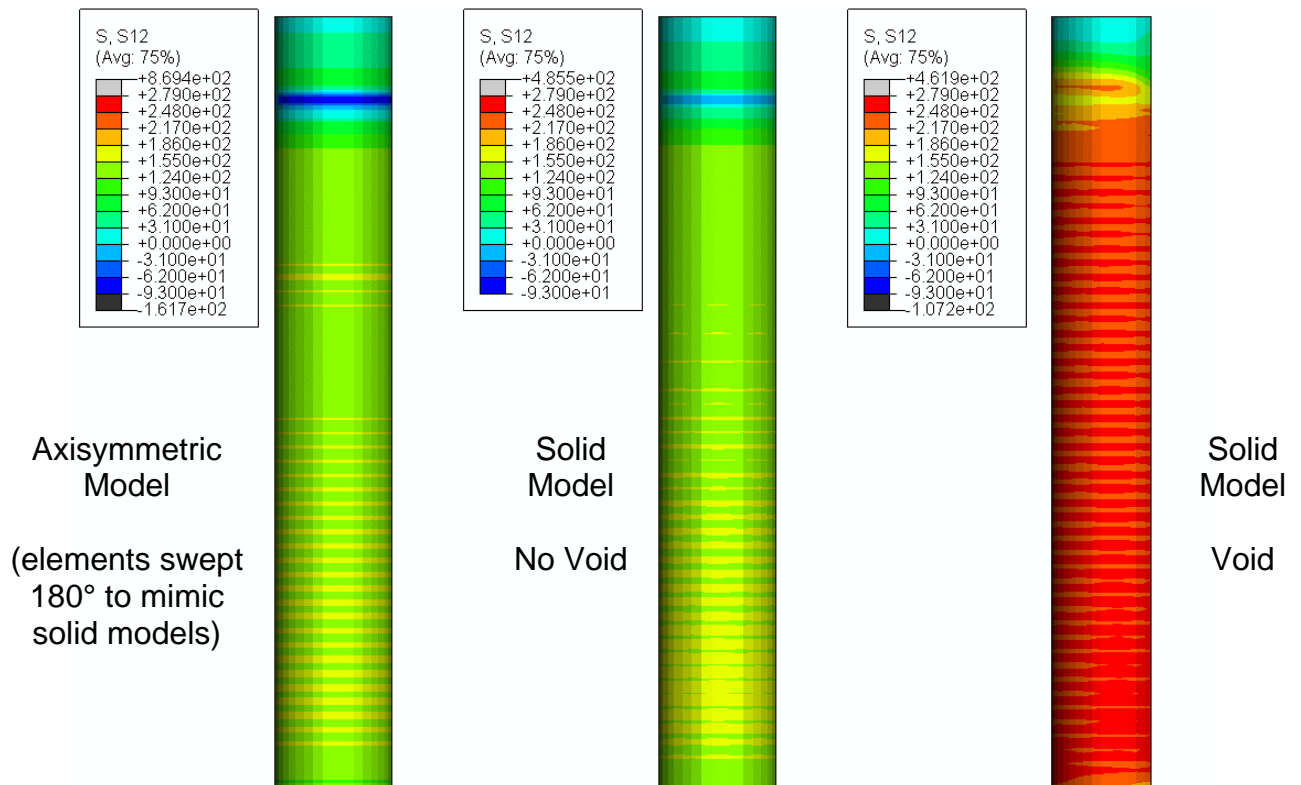


Figure 24. Contours of  $r$ - $z$  shear stress similar to figure 23, but at time step 50.

Tie Constraint

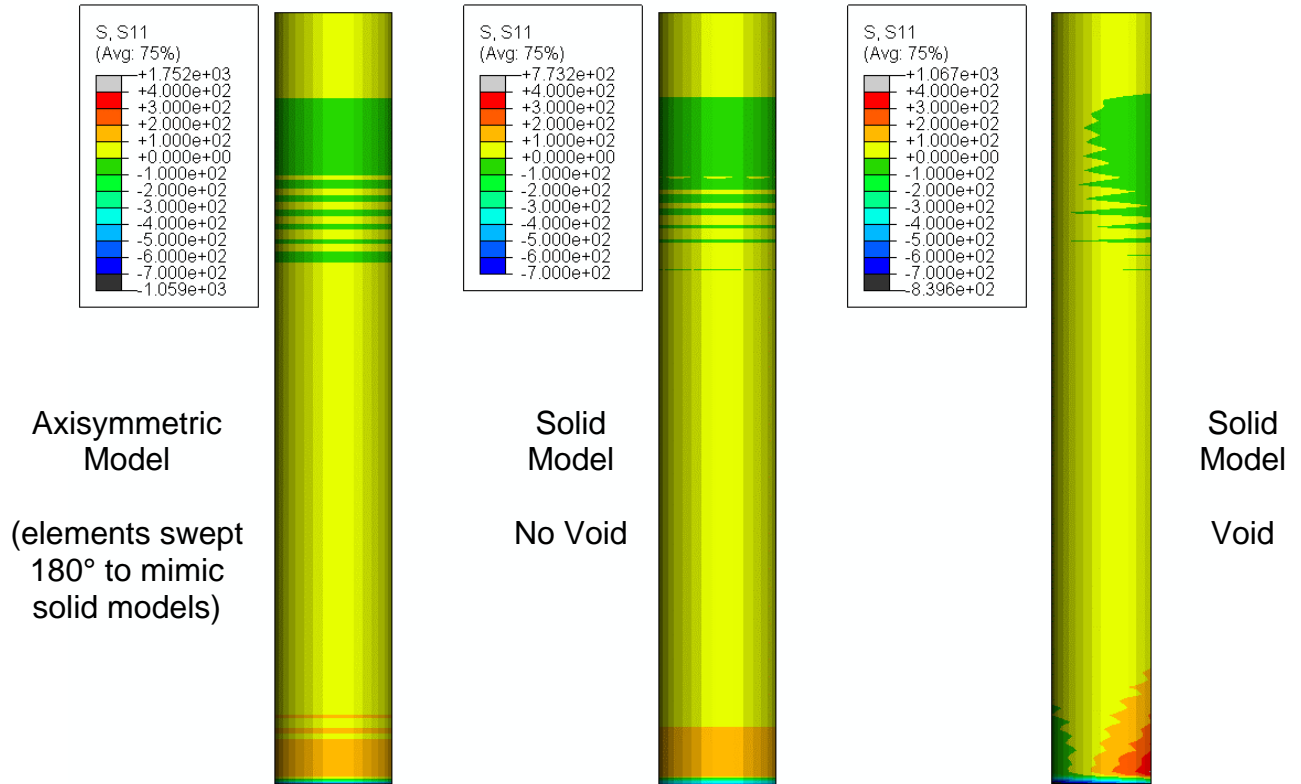


Figure 25. Contours of radial normal stress ( $\sigma_{rr}$ , in psi) at time step 1 at the epoxy surface where it bonds to the concrete, for models with a tie constraint between anchor and epoxy.

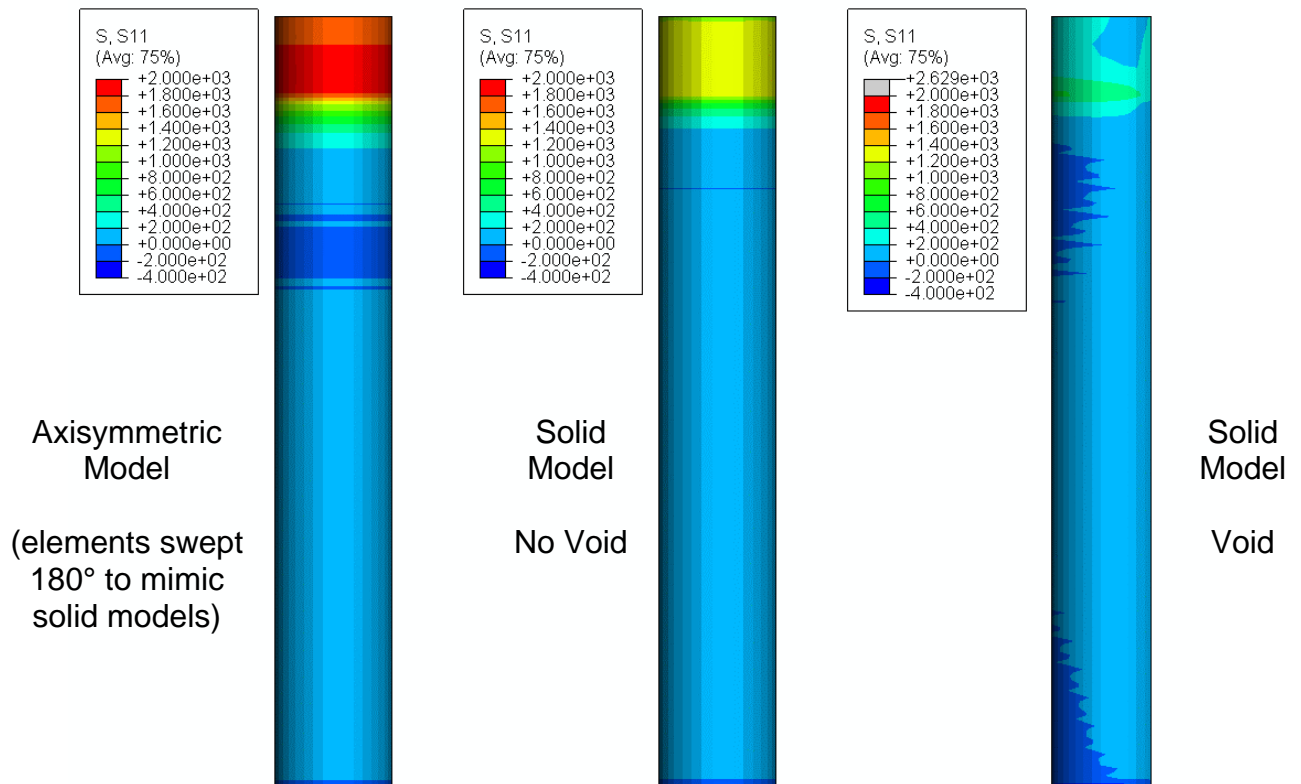


Figure 26. Contours of radial normal stress ( $\sigma_{rr}$ ) similar to figure 25, but at time step 50.

Tie Constraint

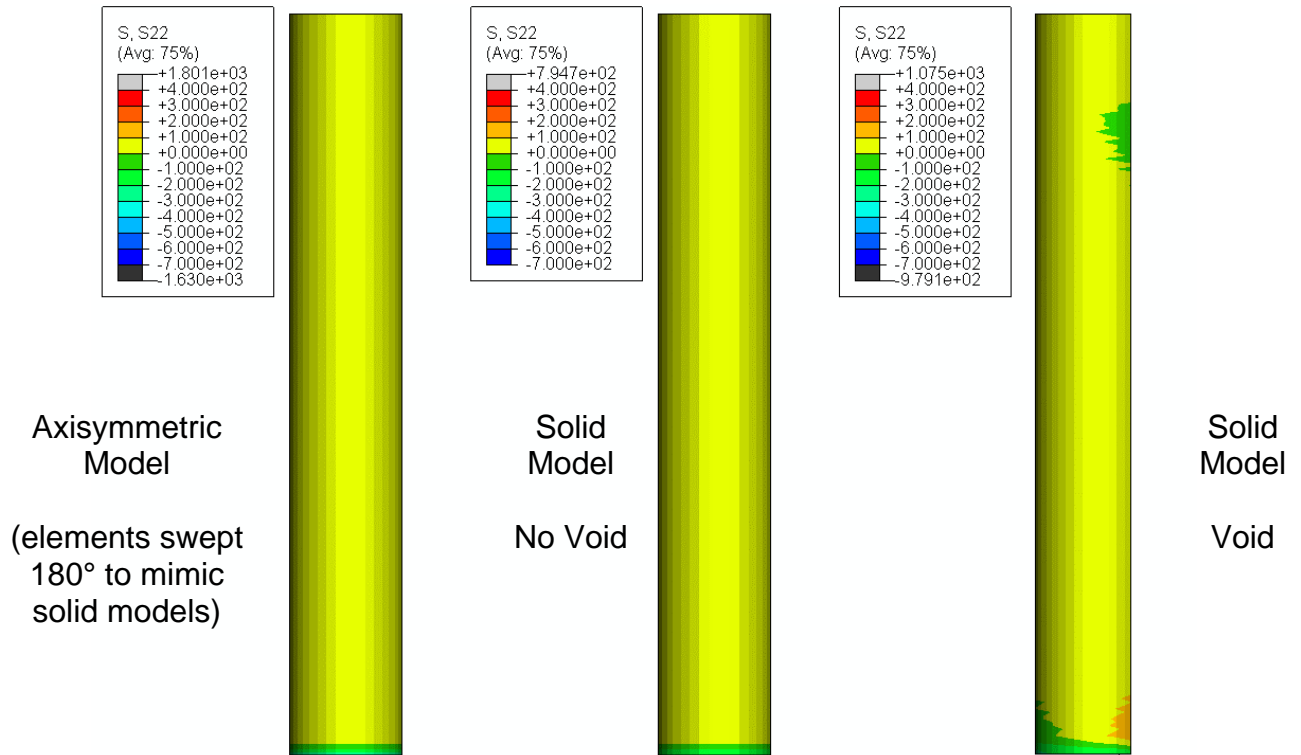


Figure 27. Contours of vertical normal stress ( $\sigma_{zz}$ , in psi) at time step 1, for models with a tie constraint between anchor and epoxy. Contour limits are the same as in figure 25.

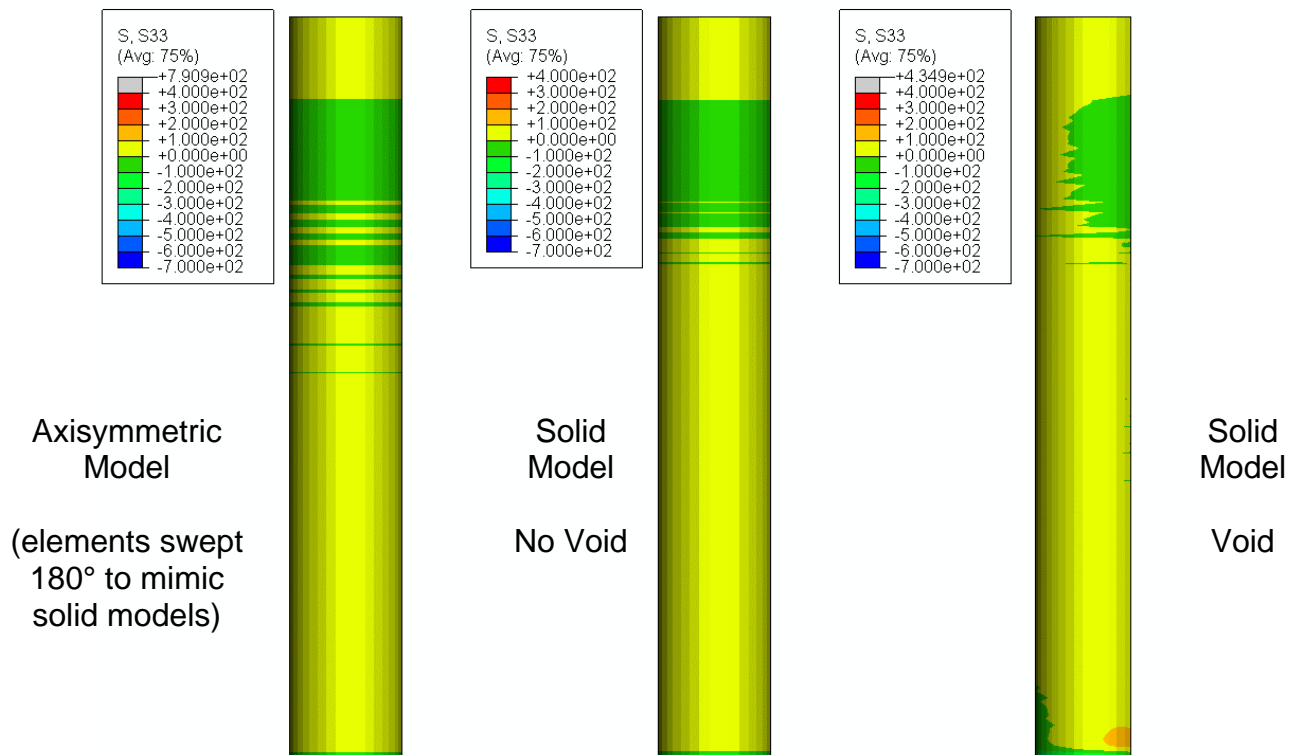


Figure 28. Contours of tangential normal stress ( $\sigma_{\theta\theta}$ , in psi) at time step 1, for models with a tie constraint between anchor and epoxy. Contour limits are the same as in figure 25.

Contact Interaction

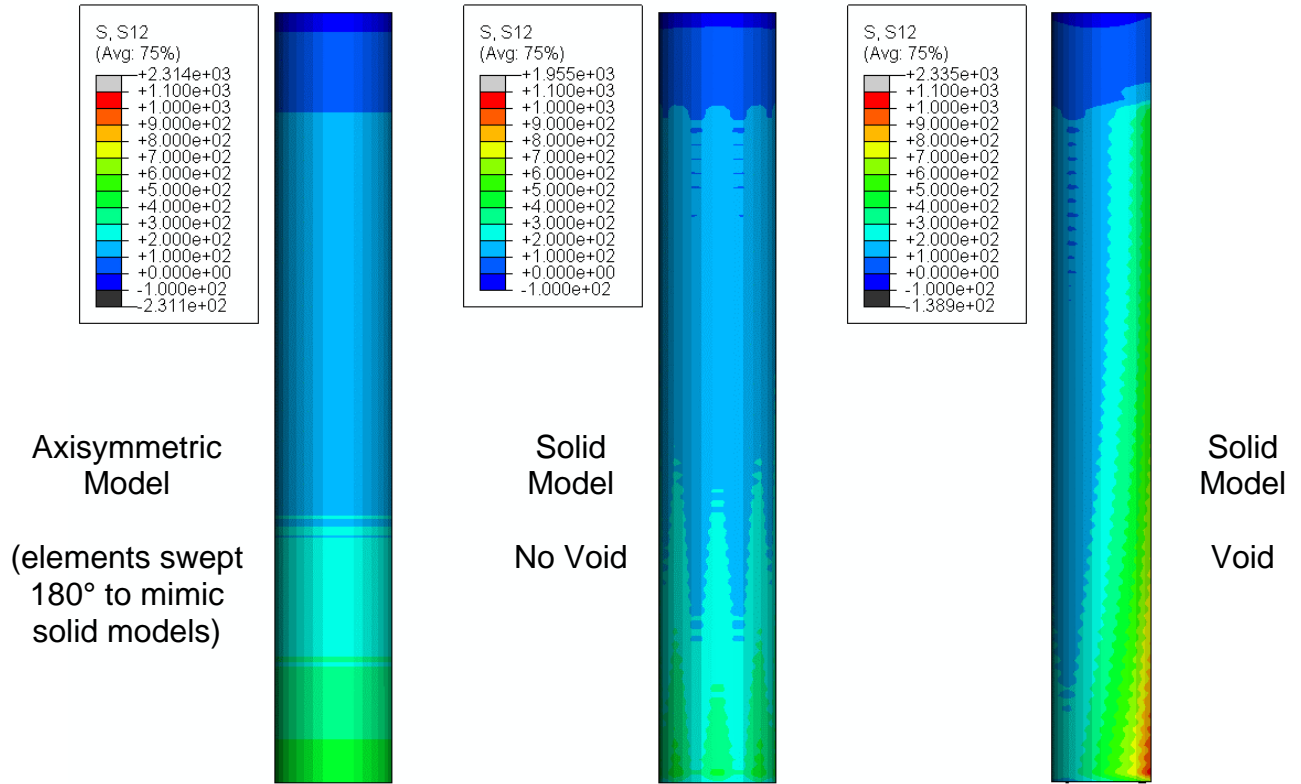


Figure 29. Contours of  $r$ - $z$  shear stress (in psi) at time step 1 at the epoxy surface where it bonds to the concrete, for models with a contact interaction between anchor and epoxy.

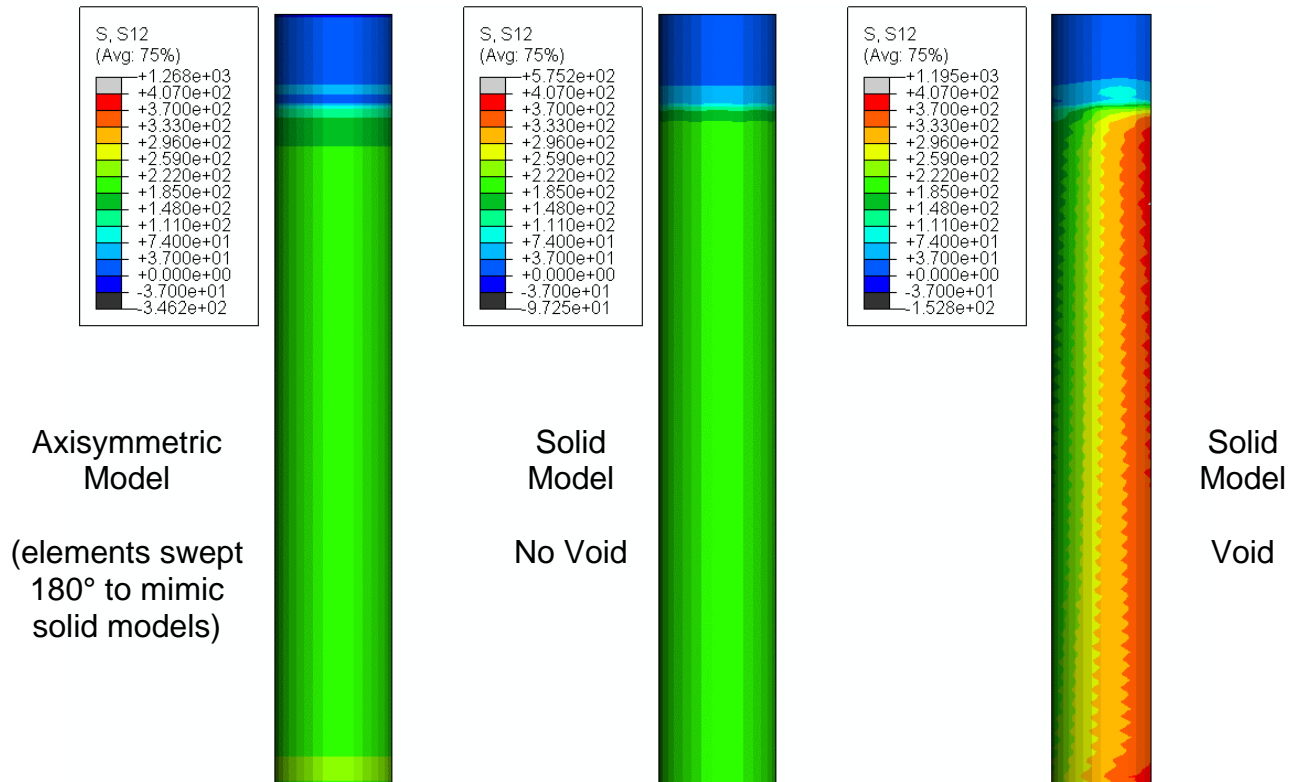


Figure 30. Contours of  $r$ - $z$  shear stress similar to figure 29, but at time step 50.

Contact Interaction

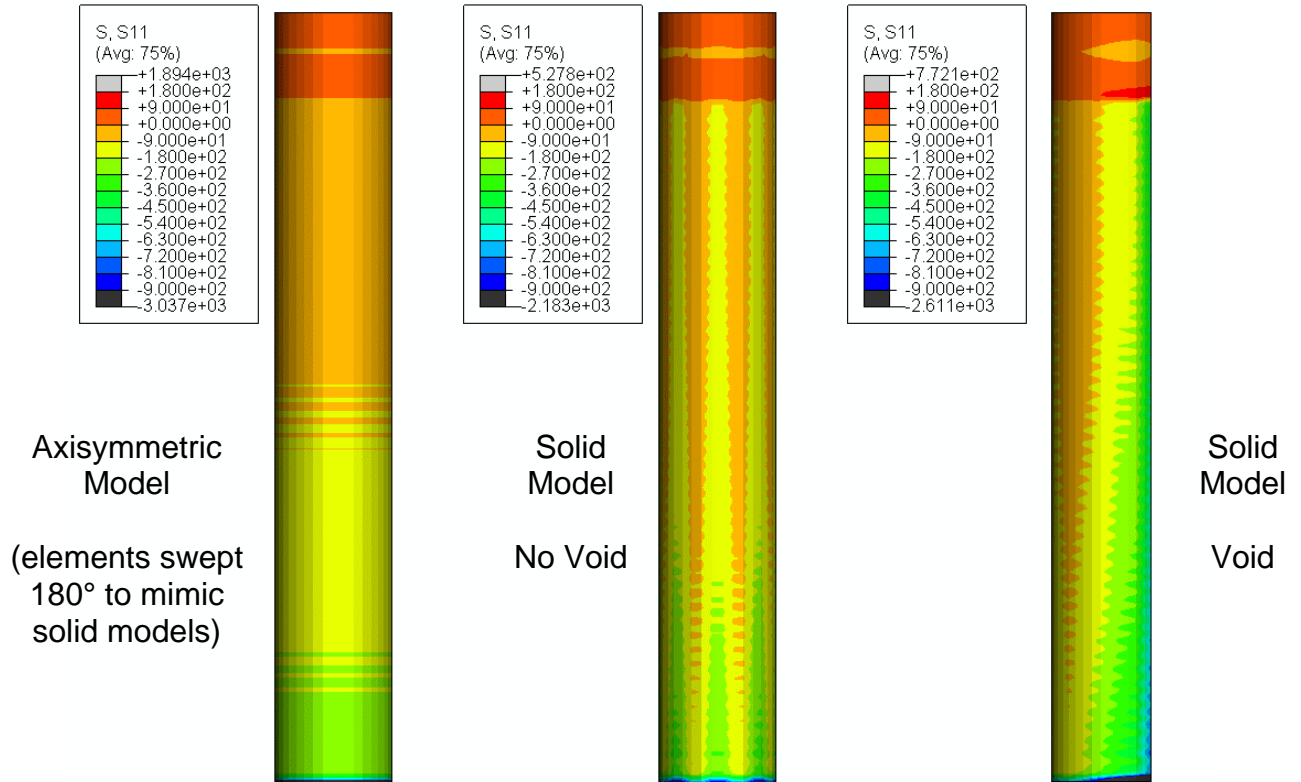


Figure 31. Contours of radial normal stress ( $\sigma_{rr}$ , in psi) at time step 1 at the epoxy surface where it bonds to concrete, for models with contact interaction between anchor and epoxy.

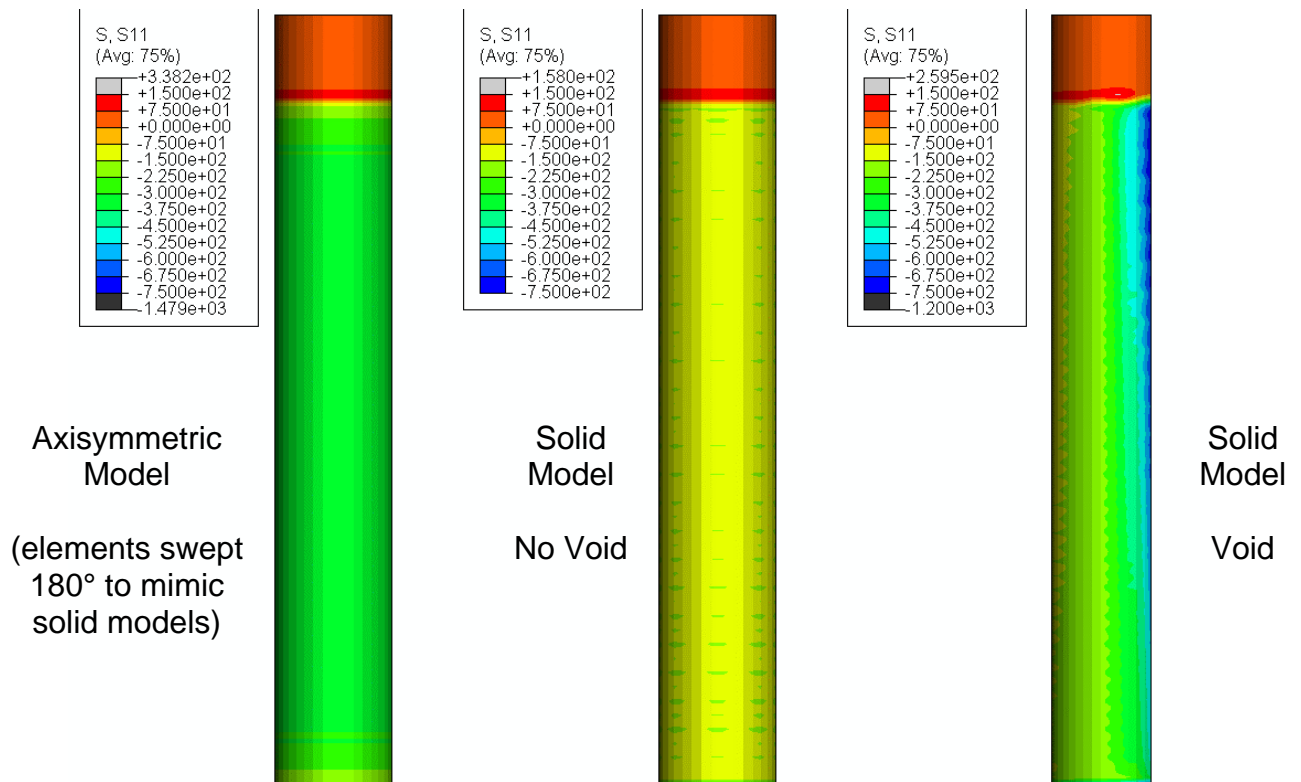


Figure 32. Contours of radial normal stress ( $\sigma_{rr}$ ) similar to figure 31, but at time step 50.

Contact Interaction

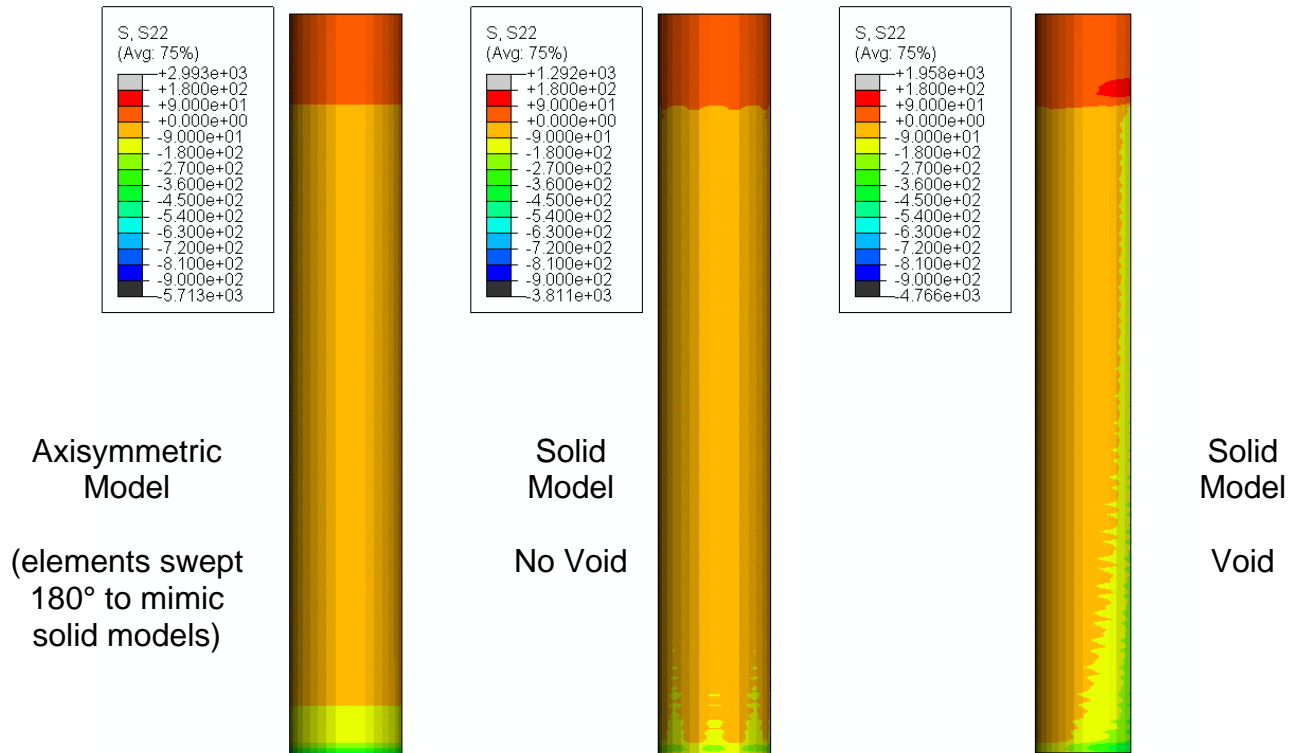


Figure 33. Contours of vertical normal stress ( $\sigma_{zz}$ , in psi) at time step 1, for models with a contact interaction between anchor and epoxy. Contour limits are the same as in figure 31.

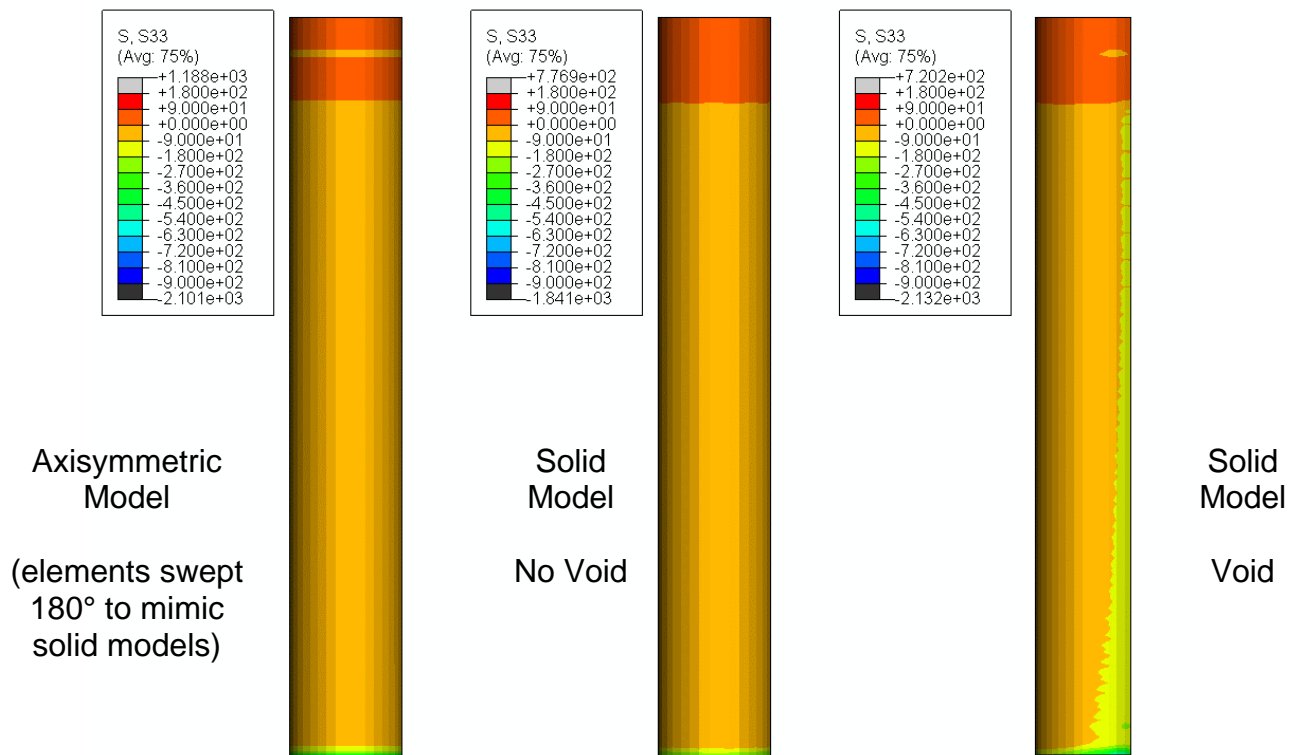


Figure 34. Contours of vertical normal stress ( $\sigma_{zz}$ , in psi) at time step 1, for models with a contact interaction between anchor and epoxy. Contour limits are the same as in figure 31.

Tie Constraint

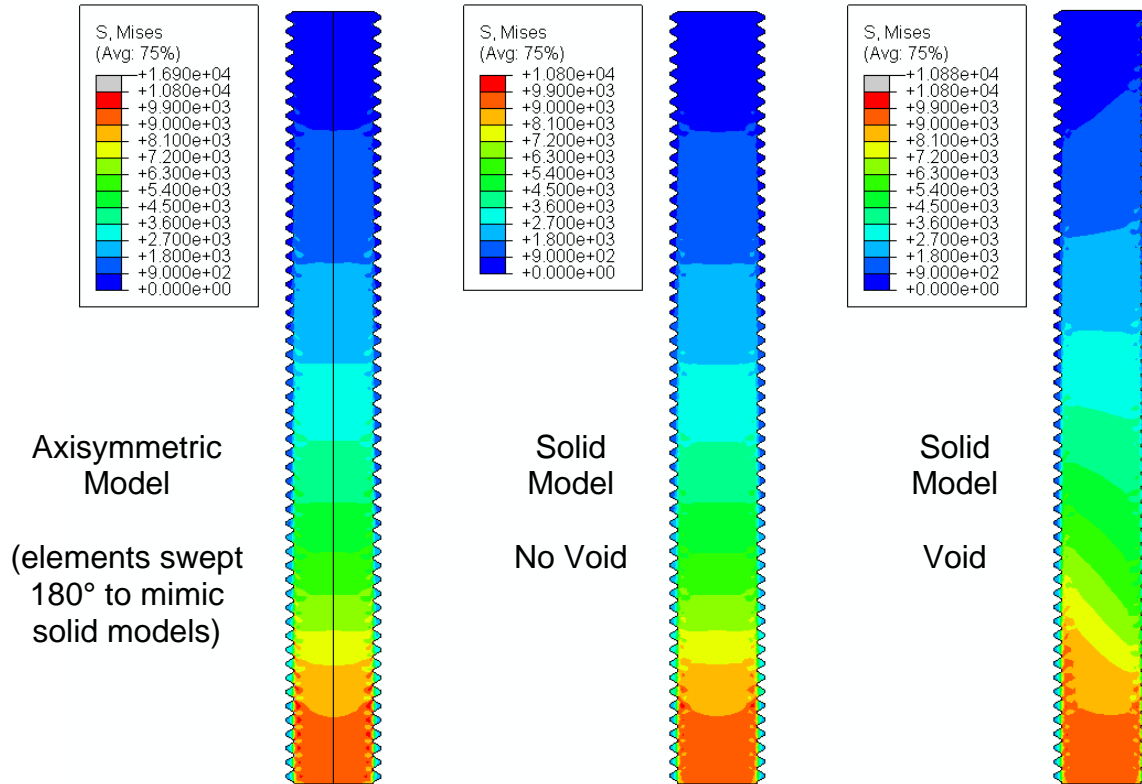


Figure 35. Contours of Von Mises stress (in psi) at time step 1 at the midplane of the anchor, for models with a tie constraint between anchor and epoxy.

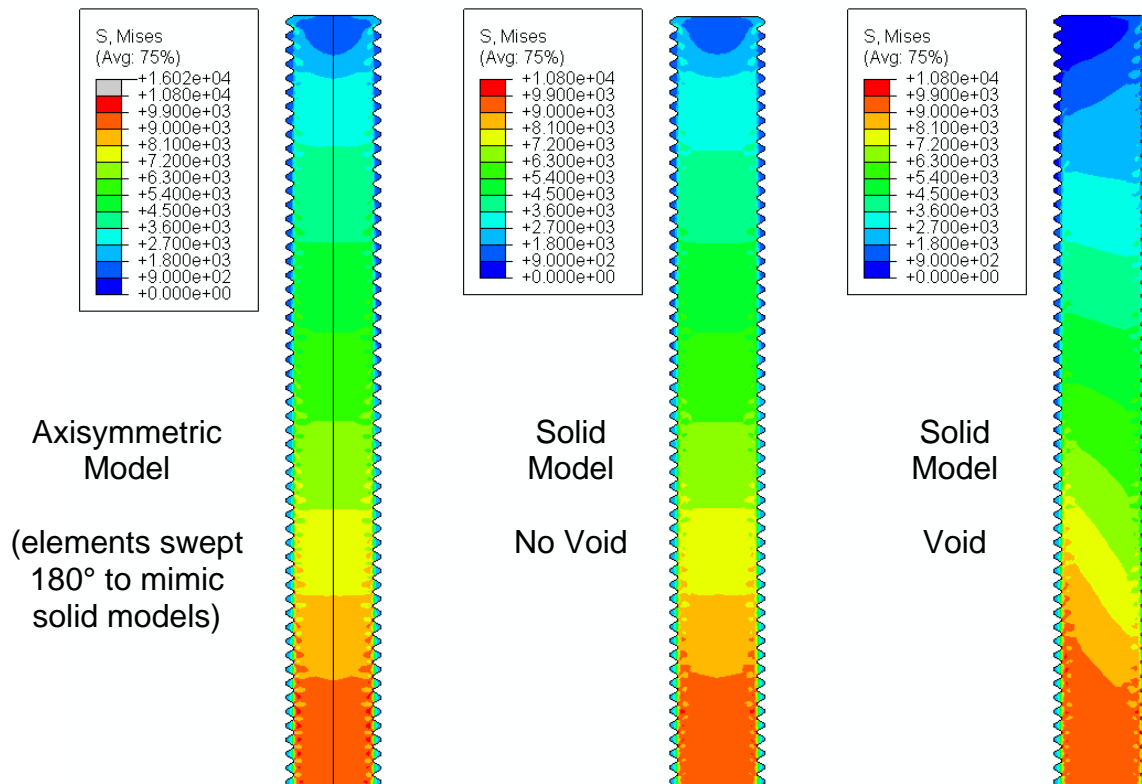


Figure 36. Contours of Von Mises stress similar to figure 35, but at time step 50.

Contact Interaction

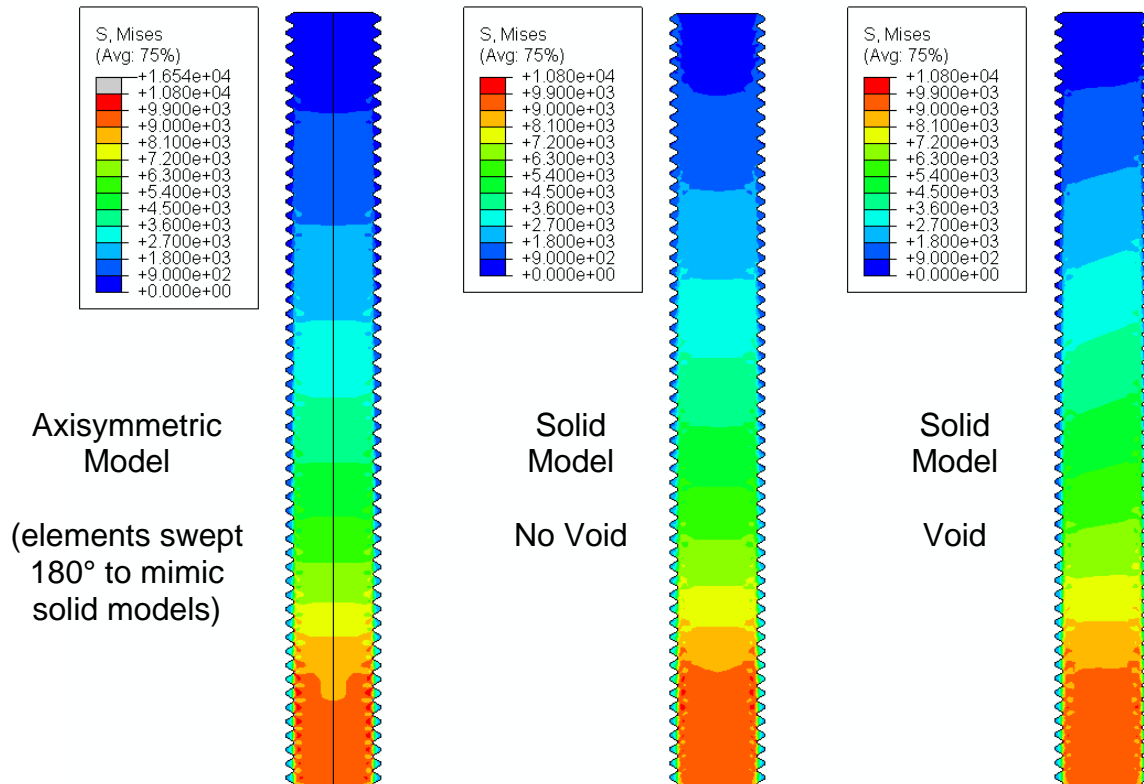


Figure 37. Contours of Von Mises stress (in psi) at time step 1 at the midplane of the anchor, for models with a contact interaction between anchor and epoxy.

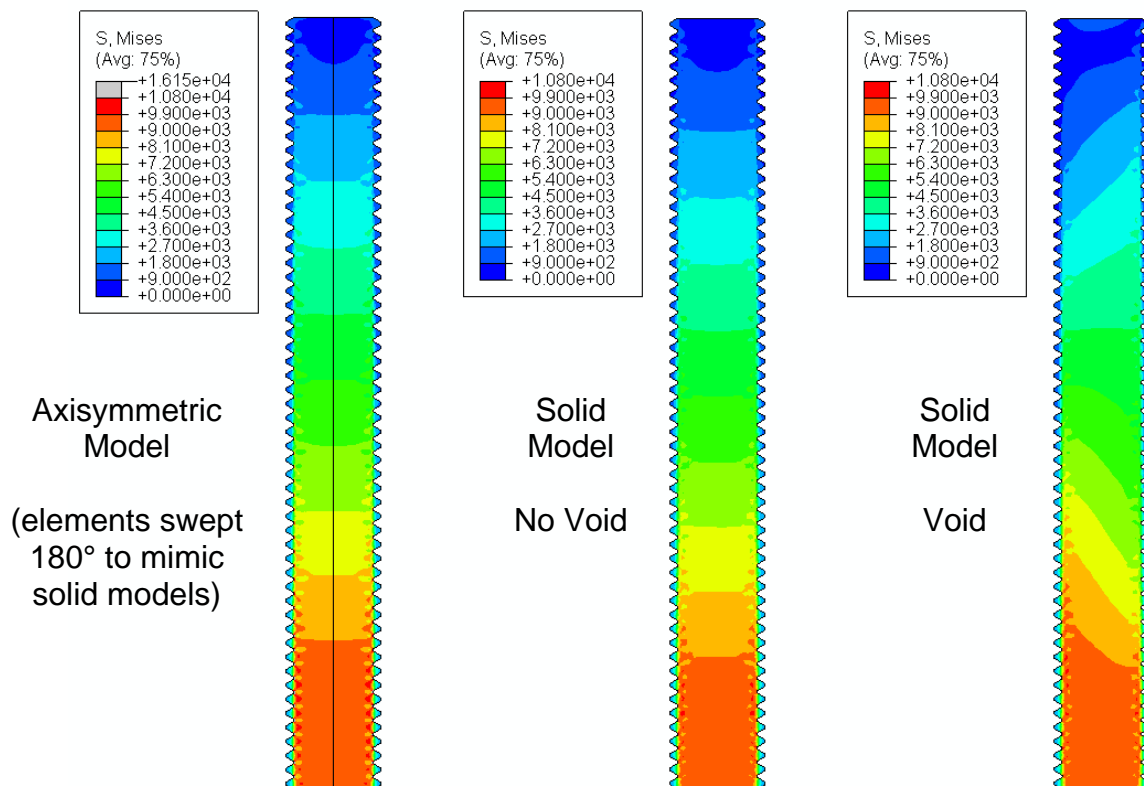


Figure 38. Contours of Von Mises stress similar to figure 37, but at time step 50.

Tie Constraint

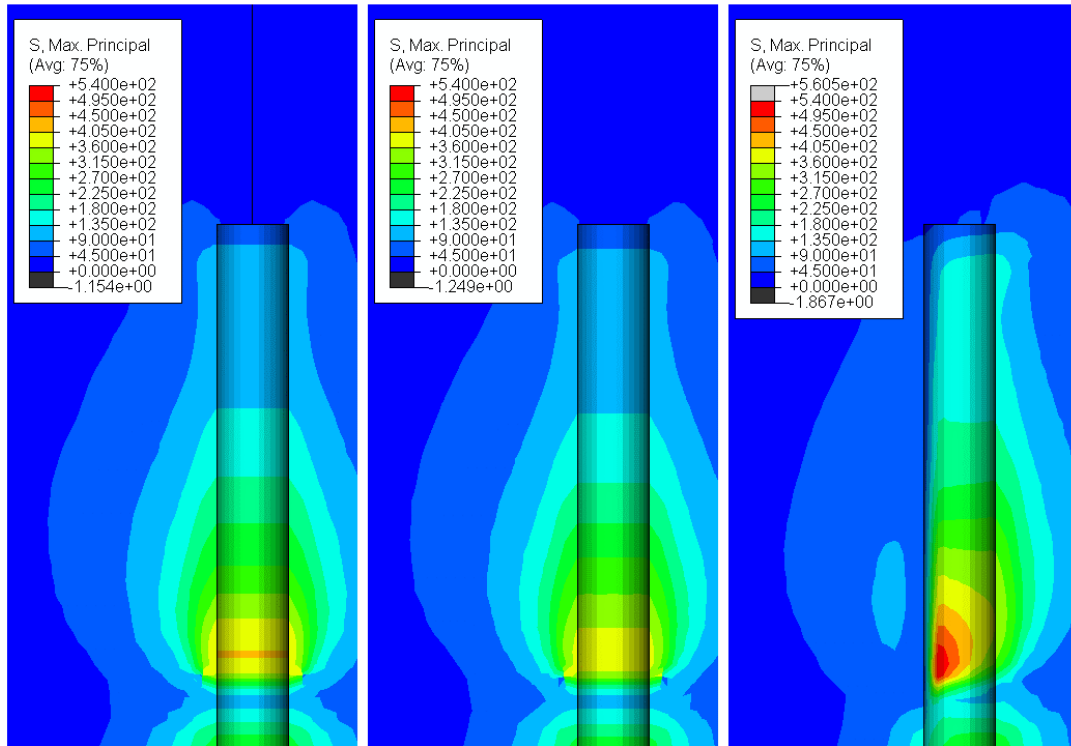


Figure 39. Contours of maximum principal stress (in psi) in the concrete cylinder at time step 1 for models with a tie constraint between anchor and epoxy. The axisymmetric model is at left (elements swept 180° to mimic solid models), the solid model with no void is in the center and the solid model with a void is at right (void is on the left side in that image).

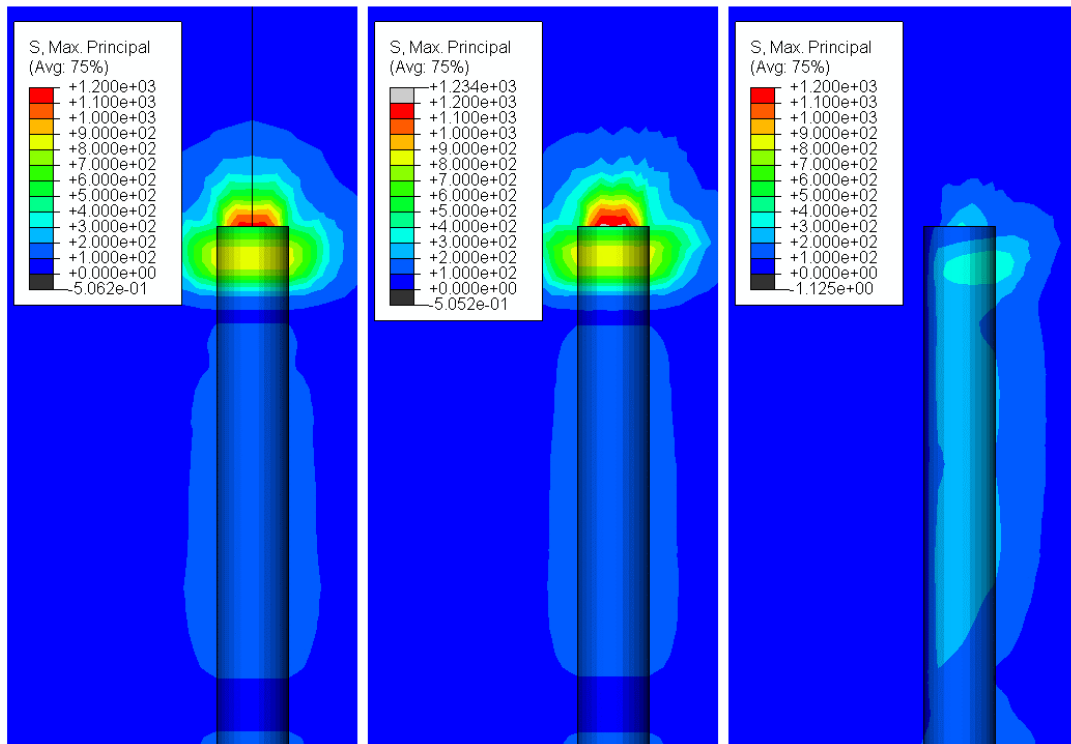


Figure 40. Contours of maximum principal stress similar to figure 39, but at time step 50.

Contact Interaction

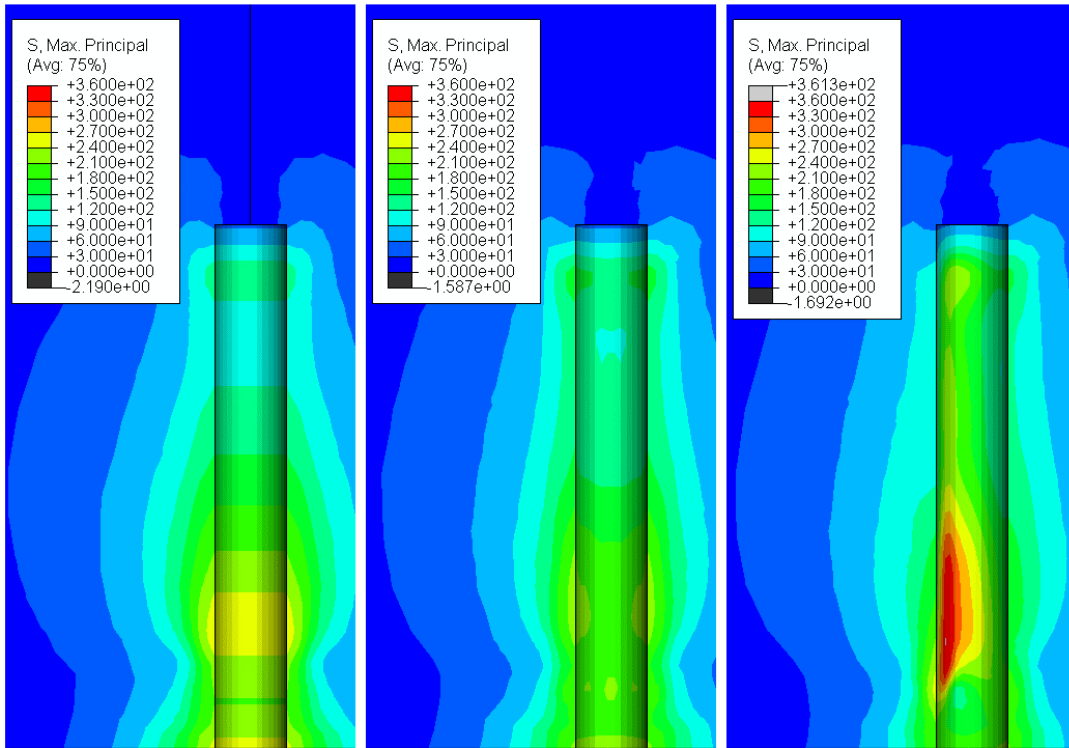


Figure 41. Contours of maximum principal stress (in psi) in the concrete cylinder at time step 1 for models with a contact interaction between anchor and epoxy. The axisymmetric model is at left (elements swept to mimic solid models), the solid model with no void is in the center and the solid model with a void is at right (void is on the left side in that image).

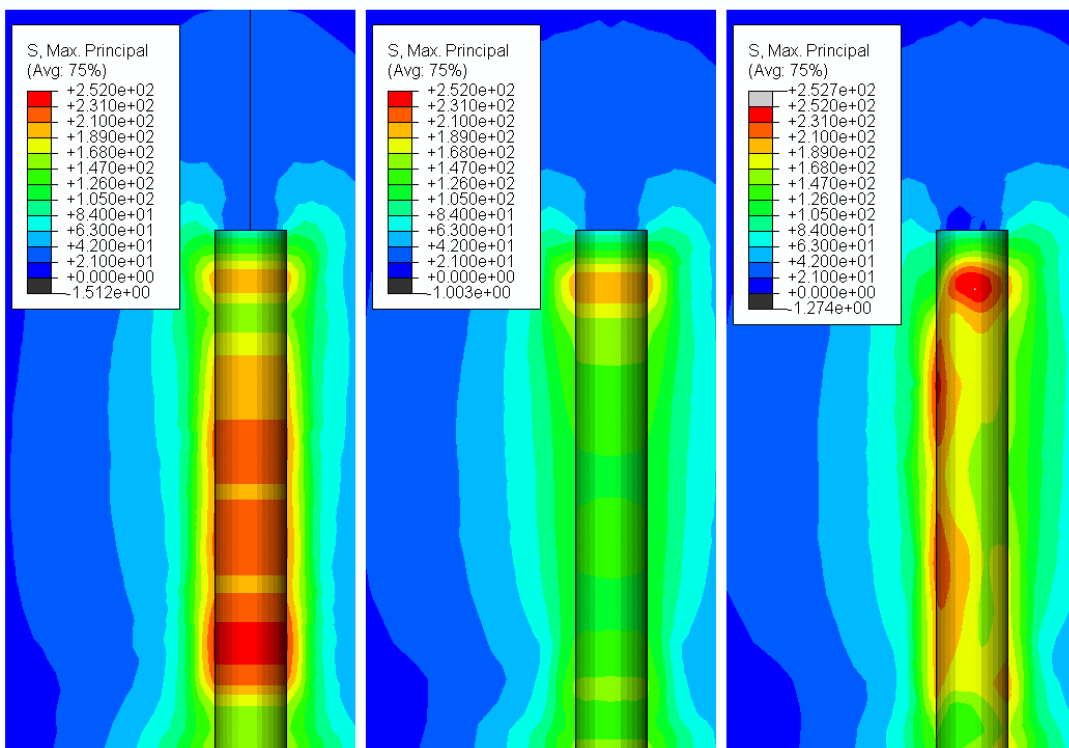


Figure 42. Contours of maximum principal stress similar to figure 41, but at time step 50.